

國立交通大學
光電工程研究所碩士班
碩士論文

IGZO 薄膜電晶體之光學
低溫退火與金屬接觸界面處理

**Development of Low Temperature Annealing and Contact
treatment by Light Illumination on Amorphous
Indium-Gallium-Zinc-Oxide (a-IGZO) Thin Film
Transistor**



研究生：黃慶能

指導教授：冉曉雯 教授

蔡娟娟 教授

中華民國九十八年七月

IGZO 薄膜電晶體之光學

低溫退火與金屬接觸界面處理

Development of Low Temperature Annealing and Contact treatment by Light
Illumination on Amorphous Indium-Gallium-Zinc-Oxide (a-IGZO) Thin Film
Transistor

研 究 生：黃慶能

Student : Ching-Neng Huang

指 導 教 授：冉曉雯 教授

Advisor : Prof. Hsiao-Wen Zan

蔡娟娟 教授

Prof. C.C. Tsai



Submitted to Institute of Electro-Optical Engineering
College of Electrical Engineering and Computer Science

National Chiao Tung University

in partial Fulfillment of Requirements

for the Degree of Master

in

Electro-Optical Engineering

July 2009

Hsinchu, Taiwan, Republic of China

中華民國九十八年七月

IGZO 薄膜電晶體之光學

低溫退火與金屬接觸界面處理

研究生:黃慶能

指導教授:冉曉雯 教授

蔡娟娟 教授

國立交通大學

光電工程研究所碩士班

中文摘要

本論文意在發展出非晶銦-鎵-鋅-氧薄膜電晶體(a-IGZO TFTs)的光學低溫退火製程。未經退火處理的 a-IGZO TFT 在在電性上的表現是很不穩定的，而後段退火處理則可以促進其在的電性上的再現性。由射頻濺鍍系統 (radio-frequency sputter) 所成長的非晶 IGZO 主動層在晶格結構上是混亂的並可能導致介電層和主動層之間載子捕捉缺陷的存在。元件操作的時候常伴隨嚴重的臨界電壓飄移現象，推測應是載子捕捉效應所造成。一般常見的退火方法為本於熱效應的高溫爐管，但其並不適合被使用在具有溫度限制的電路系統上。由本研究所發展的低溫退火技術為以脈衝雷射(Nd:YAG, 266nm) 及紫外燈(氙準分子燈, 172nm) 為光源設備，提供另外一種有別於傳統高溫爐管的退火方法。本論文中呈現，經由脈衝雷射或紫外線燈處理後的 a-IGZO TFT，其在穩定度獲得改善的同時也保有一定的元件電性，例如：載子遷移率(雷射:6.23 cm²/Vs, 紫外

燈:3.49 cm²/Vs)、臨界電壓(雷射:0.3 V, 紫外燈:0.2 V)、次臨界擺幅(雷射:0.32 V/dec., 紫外燈:0.2 V/dec.)還有開關比(10⁷), 足以和 350°C 下爐管退火後的元件相較(移動率:6.51 cm²/Vs, 臨界電壓:1.8 V, 開關比:10⁸)。除滿足低溫的訴求外, 此光學方法還可以節省時間並具有可局部化應用的能力。在連續量測下所觀察到的臨界電壓位移是一個最直接的參數來反應由載子捕捉所造成的不穩定性。未經退火的元件, 其臨界電壓的飄移量通常可達 10V 左右。脈衝雷射和紫外線燈可以有效降低臨界電壓的飄移量到 0.5 伏以下 (雷射:0.5V, 紫外燈:0V)。本篇論文之研究, 是與周政偉學長及陳蔚宗學長共同進行開發的。

在本研究中也同時證明, 使用脈衝雷射對非晶 IGZO 薄膜做表面處理將可以減少薄膜電阻率進而改善電極及主動層間的電子注入。其實, 在雷射處理後所造成的具有高導電率的 IGZO 區域已足夠直接作為源/汲極之電極, 這提供光處理之頂閘極-自對準電晶體實現的可能性。以光照射方式取代離子佈植在製程簡化或成本效率上將可具有很大的優勢。

Development of Low Temperature Annealing and Contact treatment by Light illumination on Amorphous Indium-Gallium-Zinc-Oxide (a-IGZO)

Thin Film Transistor

Student: Ching-Neng Huang

Advisor: Prof. Hsiao-Wen Zan

Prof. C.C. Tsai

Institute of Electro-Optical Engineering

National Chiao Tung University



Abstract

A low temperature fabrication method based on light illumination for amorphous Indium-Gallium-Zinc-Oxide thin film transistors (a-IGZO TFTs) was developed in this study. The as-fabricated a-IGZO TFTs without post annealing are quite unstable and demand post-annealing to get adequate repeatability in electric characteristic. The crystal structure of IGZO channel layer deposited by radio frequency sputter (rf sputter) in as-fabricated TFTs may be disorder and result in some trapping defects near interface between dielectric and active layers. Carrier trapping effect during device operation is the main source that causes instability of IGZO TFT. The general annealing method is furnace that base on thermal effect and may be not compatible with some temperature limited systems. Light illumination based on pulse laser (Nd:YAG, 266nm) or UV lamp (Xe excimer lamp, 172nm) developed in this

study provides another effective annealing approach without heating the substrate obviously. In this thesis, the stability-improved a-IGZO TFT treated by pulse laser and UV lamp also have accepted criteria, such as mobility (Laser:6.23 cm²/Vs, UV:3.49 cm²/Vs), threshold voltage (Laser:0.3 V, UV:0.2 V), subthreshold swing (Laser:0.32 V/dec. UV:0.71 V/dec.) and On/Off ratio (10⁷) which are comparable with the one annealed by 350°C furnace (mobility:6.51 cm²/Vs, V_{th}:1.8 V, subthreshold swing:0.75 V/dec. On/Off ratio:10⁸). Moreover, illumination could also be a timesaving and localizable method for further application. The threshold voltage shift during sequent transfer curve measurement is the most direct parameter to reflect the instability caused by trapping effect. The threshold voltage of as-fabricated a-IGZO TFT generally could achieve 10.8 V. Pulse laser and UV lamp annealing could reduce the threshold voltage shift to 0.5V and 0V respectively. This work was studied with my senior classmate, Cheng-Wei Chou and Wei-Tsung Chen.

This study also demonstrates that pulse laser also could be used to treat the a-IGZO surface to reduce the resistivity and then improve the carrier injection in contact. This provides an effective approach for contact treatment or even direct contact pattern. In this study, the light only patterned a-IGZO TFT perform comparable performance as compared the one with metallic contact. Therefore light illumination seems a possible method to replace ion implantation for valuable top gate self-aligned structure.

Acknowledgement

本論文能順利完成，幸得指導教授冉曉雯老師和蔡娟娟老師的指導與教誨，對於研究的方向、觀念的啟迪、架構的修正、資料的提供與求學的態度逐一教導，所以在此我獻上最深的敬意與謝意。

在研究所修業期間，我要特別感謝實驗室的博士班學長政偉學長、蔚宗學長、文元學長、士欽學長、國錫學長、彥棠學長還有武衛學長在這兩年的指導與照顧，尤其感謝政偉學長和蔚宗學長，在我這兩年的實驗上給予許多的幫助。感謝實驗室的學同學：煥之、威豪、達欣、建敏、芳弘、淑玲、繁琦、玉玫、鈞銘以及祥睿在研究上的協助和生活上的鼓勵。感謝實驗室的學弟妹：世益、琇文、建亞、明哲、翼鵬、庭毓以及唯碩，在我研究的日子裡增加了許多的歡樂。特別要感謝的是世益和琇文，不辭辛勞的幫助我做元件。使得我可以順利完成碩士論文。

家人的支持與鼓勵更是我努力的原動力。

最後，謹以此文獻給我摯愛的家人。

Contents

CHINESE ABSTRACT	I
ENGLISH ABSTRACT	III
ACKNOWLEDGEMENT	V
CONTENTS	VI
FIGURE CAPTIONS	VIII
TABLE CAPTIONS	XII
CHAPTER 1 INTRODUCTION	1
1-1 INTRODUCTION	1
1-1.1 Introduction of metal oxide transistors	1
1-2 CARRIER TRANSMISSION MECHANISM OF METAL OXIDE SEMICONDUCTORS	3
1-3 LOW TEMPERATURE ANNEALING OF METAL OXIDE TRANSISTOR	5
1-4 MOTIVATION	6
1-5 THESIS OUTLINE	8
FIGURES OF CHAPTER 1	10
CHAPTER 2 EXPERIMENTAL TECHNIQUES AND PROCEDURE	11
2-1 EXPERIMENTAL PROCEDURE	11
2-1.1 Sample preparation for annealing	11
2-1.2 Laser annealing and contact treating condition	13
2-2 OPERATION MECHANISM AND PARAMETER OF TRANSISTOR	13
2-2.1 Linear region	14
2-2.2 Saturation region	14
2-2.3 Mobility	15
2-2.4 Threshold Voltage	15
2-2.5 I _{on} /I _{off} current ratio	16
2-2.6 Subthreshold swing	16
2-3 EXPERIMENTAL INSTRUMENTS	16
2-3.1 Sputter	16
2-3.2 Electron beam evaporation	18
2-3.3 Nd:YAG LASER	18
2-3.4 Ultraviolet (UV)	19
2-3.5 Four-point probe resistivity measurement	20
FIGURE OF CHAPTER 2	22

CHAPTER 3 RESULTS AND DISCUSSIONS	26
3-1 INSTABILITY OF AS-FABRICATED A-IGZO TFTs	26
3-2 EFFECT OF POST-ANNEALING	28
3-3 I_D - V_D DIAGRAM	31
3-4 LASER INTENSITY DEPENDENCE ON A-IGZO TFTs DURING ANNEALING	33
3-5 UV INTENSITY DEPENDENCE ON A-IGZO TFTs DURING ANNEALING	35
3-6 RESULT OF CONTACT PATTERN BY LASER ILLUMINATION	36
3-7 ASSUMPTION	38
3-7.1 Mechanism of mobile carrier trapping	38
3-7.2 Physical mechanisms of channel annealing by light illumination	40
FIGURE IN CHAPTER 3	41
CHAPTER 4 CONCLUSIONS AND FUTURE WORK	60
4-1 CONCLUSIONS	60
4-2 FUTURE WORK	61
REFERENCE	62



Figure Captions

FIG. 1.1 THE OVERLAP BETWEEN THE ADJACENT ORBITALS [2].	10
FIG. 1.2 THE CARRIER TRANSPORT PATHS IN COVALENT SEMICONDUCTORS [7].	10
FIG. 1.3 THE CARRIER TRANSPORT PATHS IN AOSs [7].	10
FIG. 2.1 THE A-IGZO TFTs FABRICATION PROCESS.	22
FIG. 2.2 THE PULSE LASER TREATMENT CONTACT PROCESS.	23
FIG. 2.3 THE PULSE LASER ANNEALING SYSTEM.	23
FIG. 2.4 THE RF-POWER SPUTTERING DEPOSITION SYSTEM.	24
FIG. 2.5 THE DC-POWERED SPUTTER DEPOSITION SYSTEM.	24
FIG. 2.6 FOUR-POINT PROBE.	25
FIG. 3.1 FORWARD AND BACKWARD EIGHT TIMES SWEEPING.	41
FIG. 3.2 THRESHOLD VOLTAGE SHIFT VERSUS TEST SEQUENCE.	41
FIG. 3.3 MOBILITY VERSUS TEST SEQUENCE.	42
FIG. 3.4 SUBTHRESHOLD SWING VERSUS TEST SEQUENCE.	42
FIG. 3.5 ON CURRENT VERSUS TEST SEQUENCE.	43
FIG. 3.6 THE RECOVERY TEST (A) THE 7 TIMES MEASUREMENT TRANSFER CHARACTERISTIC FOR 0MIN AND IDLE 30MIN. (B) THE ON VOLTAGE SHIFT VERSUS MEASUREMENT SEQUENCE FOR 0MIN AND IDLE 30MIN.	44

FIG. 3.7 THE TRANSFER CHARACTERISTIC OF AS-FABRICATED A-IGZO TFTs.	45
FIG. 3.8 THE TRANSFER CHARACTERISTIC OF FURNACE ANNEALED 300°C IN N₂	45
FIG. 3.9 THE TRANSFER CHARACTERISTIC OF FURNACE ANNEALED 350°C IN N₂ A-IGZO TFTs.	46
FIG. 3.10 THE TRANSFER CHARACTERISTIC OF PULSE LASER ANNEALED A-IGZO TFTs.	46
FIG. 3.11 THE TRANSFER CHARACTERISTIC OF UV LAMP ANNEALED A-IGZO TFTs.	47
FIG. 3.12 THE (A) ABSORPTION COEFFICIENT AND (B) ABSORPTANCE OF AS-DEPOSITED IGZO AND IGZO ANNEALED BY LASER.	48
FIG. 3.13 THE OUTPUT CHARACTERISTIC DIAGRAMS FOR (A) AS-FABRICATED, (B) FURNACE ANNEALING 350°C IN N₂, (C) PULSE LASER ANNEALING AND (D) UV LAMP ANNEALING. THE V_G IS FROM 0.1 V TO 20.1 V AND STEP IS 10 V.	49
FIG. 3.14 THE TRANSFER CHARACTERISTIC WITH DIFFERENT PULSE LASER ENERGY DENSITY TREATMENT (10.02~29.71 mJ/cm²).	50
FIG. 3.15 THE SHEET RESISTANCE WITH DIFFERENT PULSE LASER ENERGY DENSITY.	50
FIG. 3.16 THE TRANSFER CHARACTERISTIC WITH DIFFERENT PULSE LASER ENERGY TREATMENT AFTER FURNACE ANNEALING 400°C, O₂ FLOW 120 SCCM, PRESSURE 0.3TORR AND 1HOUR.	51
FIG. 3.17 THE TRANSFER CHARACTERISTIC WITH DIFFERENT UV LAMP ILLUMINATION TIME (10~180 MIN).	51

FIG. 3.18 THE SHEET RESISTANCE WITH DIFFERENT UV LAMP ILLUMINATION TIME (10~30 MIN).	52
FIG. 3.19 THE TRANSFER CHARACTERISTIC WITH DIFFERENT PULSE LASER ENERGY TREATMENT AFTER FURNACE ANNEALING 400°C, O₂ FLOW 120 SCCM, PRESSURE 0.3TORR AND 1HOUR.	52
FIG. 3.20 THE FLOW CHARTS THAT PRESENT THE LIGHT PATTERN PROCEDURE. SAMPLE (A) REPRESENT THE SOURCE/DRAIN CONTACTS WERE PATTERNED BY PULSE LASER ILLUMINATION DIRECTLY OF THE FIRST A-IGZO TFTs. SAMPLE (B) EQUIPPED WITH TI PADS ON THE AREA TREATED BY PULSE LASER PREVIOUSLY TO FORM THE SOURCE/DRAIN CONTACT. TI PADS SERVE AS SOURCE/DRAIN CONTACTS IN THE THIRD IGZO TFT WHICH DENOTED BY SAMPLE (C).	53
FIG. 3.21 THE TRANSFER CHARACTERISTIC OF SAMPLE (A), (B) AND (C).	54
FIG. 3.22 THE OUTPUT CHARACTERISTIC OF SAMPLE (A), (B) AND (C).	55
FIG. 3.23 THE TRAPPING MECHANISM OF AS-FABRICATED A-IGZO TFTs. (A) THE POSITIVE V_G THAT CAUSE ELECTRON TRAPPING BETWEEN SiN_x/A-IGZO INTERFACE. (B) AFTER REMOVE THE BIAS, THE TRAPPED ELECTRONS WERE STILL NOT RELEASED. (C) DURING NEXT MEASUREMENT, THE LARGER POSITIVE GATE VOLTAGE IS REQUIRED TO FLAT THE CONDUCTION BAND.	56
FIG. 3.24 THE UN-OCCUPIED DEFECTS THAT WILL MAKE THRESHOLD SHIFT AND LOWER	



Table Captions

TABLE 2.1 LASER INTENSITY CONDITIONS.	25
TABLE 3.1 THE PARAMETERS OF DIFFERENT POST-ANNEALING CONDITIONS	58
TABLE 3.2 THE PARAMETERS OF DIFFERENT PULSE LASER ENERGY DENSITY	58
TABLE 3.3 THE PARAMETERS OF DIFFERENT UV LAMP ILLUMINATION TIME	59
TABLE 3.4 THE PARAMETERS OF DIFFERENT UV LAMP ILLUMINATION TIME	59



Chapter 1

Introduction

1-1 Introduction

1-1.1 Introduction of metal oxide transistors

Metal oxide semiconductor was first reported in 1964 by H. A. Klasens et.al. [1]

The material of metal oxide composed of heavy metal cations with an electronic configuration $(n - 1)d^{10} ns^0$ ($n \geq 4$) are promising candidate for next generation semiconductor. [2] These ns orbitals have large radius, so that there is a large overlap between the adjacent orbitals shows in Fig. 1.1. Over the past few years, several oxide materials are reported to be the channel material in TFTs. The polycrystalline zinc oxide (ZnO)[3,4], amorphous zinc tin oxide (ZTO) [5], amorphous zinc indium oxide (ZIO)[6], and amorphous indium gallium zinc oxide (IGZO)[7-9] are proposed to be the active layer in transparent TFTs. Among the transparent oxide channel materials, amorphous indium gallium zinc oxide (a-IGZO) applied to thin film transistors (TFTs) has drawn considerable attention due to their high mobility, good transparency, and unique electrical properties. [10,11] Moreover, the amorphous type of a-IGZO was insensitiveness to the distorted metal–oxygen-metal chemical bonds. [2] Large band gap ($>3\text{eV}$) induces that the a-IGZO material was insensitive to the ambient light and transparent in visible region (400nm~700nm). The carrier concentration ($n: 10^{13} \sim 10^{20}$)

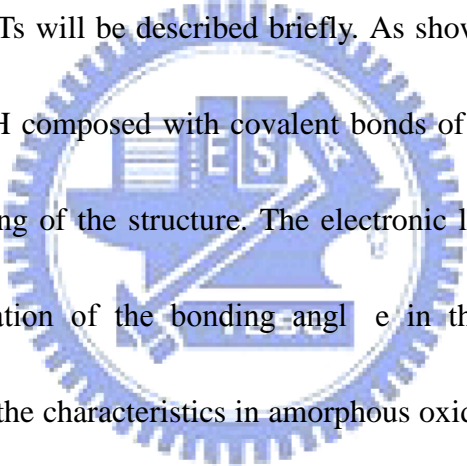
cm^{-3}) in the a-IGZO film was tunable by controlling the oxygen pressure during film deposition.

When a-IGZO TFTs is applied to temperature limited substrates like flexible substrate, the radio-frequency (rf) sputtering technique is one of a few methods which enables us to deposit thin films of high-melting-temperature materials over large areas at low substrate temperatures. [12] However, H. Hosono et al. proposed that the chemical species and/or a structure in a thin film are naturally unstable when thin films are deposited at low temperatures. [12,13] Additionally, they are stable while thin films are deposited at higher temperatures. The chemical species and/or a structure are frozen in the as-deposited thin film which relax to a more stable state and /or give the atoms more energy to rearrange upon thermal annealing, leading to an appreciable change in the electron transport properties. [12,13] Most oxide TFTs, especially a-IGZO TFTs, are fabricated using physical vapor deposition (PVD) techniques at room temperature and often require a high temperature post-deposition thermal annealing process to get high-performance and high-stability TFTs. [12-18] Among the post-deposition thermal annealing techniques, rapid thermal annealing (RTA) [16,17] or furnace annealing [18] are usually used to anneal the oxide TFT devices. For the application of a-IGZO TFTs which is fabricated on the temperature limited flexible substrate, high temperature thermal annealing may damage the

substrates. Development of the annealing method at low substrate temperature is essential when applying a-IGZO TFTs to flexible and temperature limited substrates

1-2 Carrier transmission mechanism of metal oxide semiconductors

The mechanism of carrier transmission in amorphous oxide semiconductor, a-IGZO, was discussed in this section. Before reporting the a-IGZO mechanism, the hydrogenated amorphous silicon (a-Si:H) transmission mechanism, the conventional material for flexible TFTs will be described briefly. As shown in Fig. 1.2, the carrier transport paths in a-Si:H composed with covalent bonds of sp^3 orbitals was affected obviously by the ordering of the structure. The electronic levels and trap states was influenced by the fluctuation of the bonding angle in the a-Si:H structure. [19]

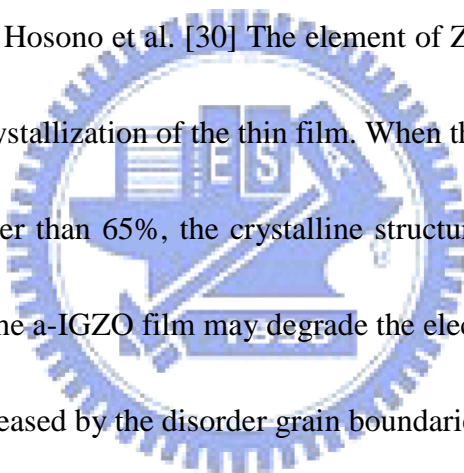


Compare to the a-Si:H, the characteristics in amorphous oxide semiconductors (AOSs) are different from the semiconductors with covalent bonds. The carrier-transport path in AOSs was shown in Fig. 1.3. The bottom of the conduction band in the oxide semiconductors that has large ionicity is primarily composed by spatially spread metal ns (here n is the principal quantum number) orbitals with isotropic shape. [19] There were no conduction paths formed by the 4s orbitals had been obtain so far in any amorphous oxide. Based on these facts, the condition necessary for good conductivity in a-IGZO is that the conduction paths should be composed of the ns orbitals. The

principal quantum number is at least 5 [20] and direct overlap among the neighbor metal ns orbitals is possible. The magnitude of this overlap is insensitiveness to distorted metal–oxygen–metal (M–O–M) chemical bonds that intrinsically exist in amorphous materials. [21,22] The amorphous oxide semiconductors (AOSs) containing post-transition-metal cations was possible to show the degenerate band conduction and high mobility ($>10 \text{ cm}^2/\text{Vs}$). [20,23]

Each sub-element in this ternary material of a-IGZO film showed various characteristics to affect the parameters of TFTs. Higher concentration of In atom is expected to generate high carrier. [24] The element of In is a big atom and easy to lose electrons while the oxygen is a small atom and easy to get electrons from the In. The released electron from the element of In may move to the conduction band when the composition of a-IGZO lacked for oxygen. [25] It will enhance the carrier transport during the operation in TFTs. In addition, the element of Ga was introduced provide high stability in a-IGZO TFTs. [26] The element of Ga in the a-IGZO film was introduced to reduce the electron concentration, mobility. The Ga was chosen because of atomic radius of Ga closed to In. Hosono et al. reported that the Ga^{3+} in the a-IGZO film attract the oxygen tightly due to the high ionic potential resulted from the small ionic radius and +3 valence. It suppresses the electron injection and induces the oxygen ions escaping from the a-IGZO film. [27] Compare to the carrier

concentration in the material of IZO ($\sim 10^{21} \text{ cm}^{-3}$), smaller carrier concentration of a-IGZO ($\sim 10^{19} \text{ cm}^{-3}$) is reported. [20, 27-29] Ga also reduces the sensitivity of the carrier concentration when the O_2/Ar ratio is varied. [29] Introducing the element of Ga to the a-IGZO film helps the carrier concentration of the a-IGZO film to be controlled easily. However, the mobility reduced while the Ga was introduced to the a-IGZO film. Doping the oxygen molecules to increasing the carrier concentration and the carrier mobility when the element of Ga was introduced the a-IGZO film which was proposed by Hosono et al. [30] The element of Zn in the a-IGZO film was reported to affect the crystallization of the thin film. When the ratio of the Zn atoms in the a-IGZO film is larger than 65%, the crystalline structure was reported. [25] The crystalline structure in the a-IGZO film may degrade the electrical characteristic while the uniformity was decreased by the disorder grain boundaries.



1-3 Low temperature annealing of metal oxide transistor

In last section we reported that Hosono et al. proposed the chemical species and/or a structure in a thin film are naturally unstable when thin films are deposited at low temperatures. [12,13] They are stable while thin films are deposited at higher temperatures. The chemical species and/or a structure are frozen in the as-deposited thin film which relax to a more stable state and/or give the atoms more energy to rearrange upon thermal annealing, leading to an appreciable change in the electron

transport properties. The a-IGZO TFTs, are fabricated using PVD techniques at room temperature required a high temperature post-annealing process to get high-performance and high-stability TFTs. [12-18] Among the post-annealing techniques, rapid thermal annealing (RTA) [16,17] or furnace annealing [18] are often used to anneal the oxide TFT devices. In order to the application of a-IGZO TFTs which is fabricated on the temperature limited flexible substrate, high temperature thermal annealing may damage the substrates. Development of the annealing method at low substrate temperature is essential when applying a-IGZO TFTs to flexible and temperature limited substrates. To solve this problem, we lead into the laser and UV annealing method to get an overall low temperature process even at room temperature. In this thesis, we reported the laser and UV post-annealing method help to improve the performance of a-IGZO TFTs that can compare with the furnace annealing. Nakata et al. reported that the laser annealing at low substrate temperature improved the performance of a-IGZO TFTs [31]. The wavelength of the laser used to anneal the a-IGZO TFTs was 308nm. The bandgap of the a-IGZO film was around 3.2 eV. It means that the wavelength of the UV area was easy to be absorbed by the a-IGZO film.

1-4 Motivation

To fabricate high performance low temperature a-IGZO TFTs on temperature

limited substrate. The annealing methods using light illumination were proposed in this paper. The photon energy of employed light source was larger than the bandgap of a-IGZO. High energy photons can be absorbed effectively by the a-IGZO film. The light sources proposed to anneal the a-IGZO film at low substrate in this thesis were Nd:YAG pulse laser (266nm) and Xe excimer lamp (172nm). By applying these simple and convenient annealing methods, it is possible to fabricate high stability flexible transparent electrical devices on some temperature limited substrates, such as flexible substrates.

Ahn et al. reported that laser annealing at the high energy density lower the sheet resistance of the film. [32] The laser annealing at high density is proposed to reduce the contact resistance in the metal-semiconductor interface which between the source-drain (S/D) electrodes and a-IGZO. It is crucial to achieve high-performance TFTs. The most research of a-IGZO TFTs have focused on fabricating process variables such as the chemical components, oxygen partial pressure, deposition power of the IGZO target and processing techniques [33,34]. Recently, two researches reported the effect of argon (Ar) plasma treatment on the contact resistance in bottom gate [35] and top gate [36] a-IGZO TFTs. We follow the ideal of post-treatment to reduce the contact resistance and use the LASER to replace the Ar plasma. If it was employed on self-aligned structure that can minimize the parasitic capacitance by

reducing the gate overlap and eliminates the contact resistance between the electrode and channel layer. [37] The major loss of the device performance is often due to the presence of high resistance metal-semiconductor interface. A poor interface between the a-IGZO channel and gate dielectric leads to large interface trap density and reduced carrier transport properties. It causes a degradation of device parameters such as leakage current, saturation mobility and subthreshold swing. [38] Light pattern treatment can overcome these problems and improve these drawbacks.

For the achievement of flexible displays, it would be extremely helpful to fabricate high performance a-IGZO TFTs at substrate with temperatures less than 150 °C. Laser [30] and ultraviolet (UV) illumination are the appropriate method for low temperature post-annealing, it can help to fabricate the device on temperature limited substrate. This method not only can use in the temperature limited substrate, but also can get the similar performance just as after furnace annealing.

1-5 Thesis outline

In chapter 1, we brief introduced advantage and potential of a-IGZO based transistor compare with a-Si material. Then we also reported the benefit of low temperature post-annealing and used laser to reduce the contact resistance. The theoretical of carrier transmission mechanism of metal oxide semiconductor and specific property of a-IGZO in metal oxide based semiconductor for each sub-element

also report in this section.

In chapter 2, introduce the experimental procedure, like device preparation, laser annealing, contact treating condition and how to extract the characteristic parameter.

Then overview the experimental equipment such as sputter, E-beam, Nd-YAG LASER and four-point probe resistivity measurement.

In chapter 3, the main point of this thesis we study the results of low temperature post-annealing and discuss the phenomenon after annealing.

In chapter 4, make a conclusion of our experiments and future work.



Figures of Chapter 1

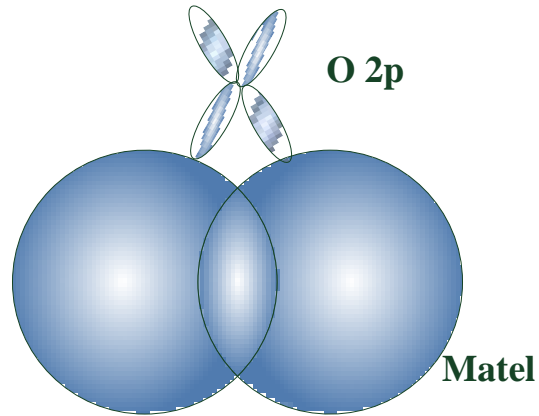


Fig. 1.1 The overlap between the adjacent orbitals [2].

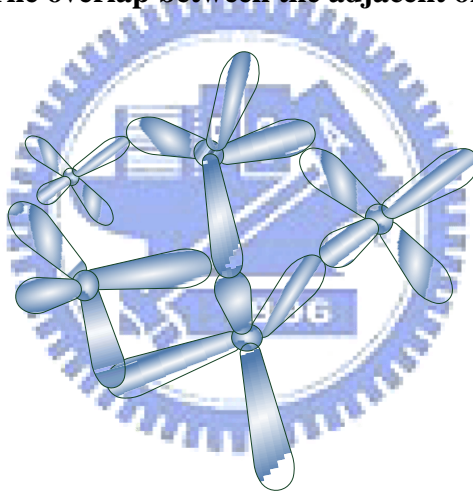


Fig. 1.2 The carrier transport paths in covalent semiconductors [7].

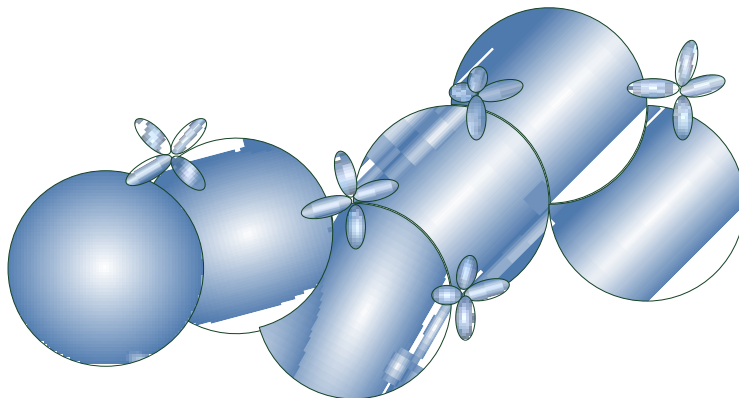


Fig. 1.3 The carrier transport paths in AOSs [7].

Chapter 2

Experimental Techniques and procedure

2-1 Experimental procedure

In this section, the device structure and the process flow of the a-IGZO based TFTs on the SiN_x dielectric were demonstrated. As described in section 2-2.1, the top contact structure of the a-IGZO layer was patterned on the SiN_x surface using the shadow mask. In section 2-2.2, the laser treatment condition and structure will show.

The detail fabrication processes are listed as following sections:

2-1.1 Sample preparation for annealing

1. Substrate and gate electrode

As shown in Fig. 2.1, a 6-inch p-type heavily-doped single crystal silicon wafer is used as substrate and gate electrode for fabricating a top-contact bottom-gate based TFTs.

2. Deposition of the SiN_x dielectric

1000Å silicon nitride (SiN_x) formed the dielectric layer in order to fabricate the a-IGZO TFTs device. The SiN_x film was deposited on all samples using low pressure chemical vapor deposition (LPCVD) at 780 °C with the NH_3 and SiH_2Cl_2 reactant gas. The silicon nitride formed on the back of the silicon substrate was etched by the ion etching (RIE). Before etching SiN_x , the FH-6400 photo resist was spin-coating on the

front of silicon wafer to protect the dielectric surface. To remove the SiN_x from the back of silicon wafer, the RIE system required the reactant gas, including the oxygen (O_2) 5 sccm and CF_4 80 sccm. The working pressure of 15.0 Pa and the RF power of 100W were controlled to etch the SiN_x film. After the RIE process, the clean process of the SC1 and SC2 was required to clean the wafer.

3. Deposition of the a-IGZO film

After the SiN_x films were deposited and cleaned, the a-IGZO film (In:Ga:Zn=1:1:1) was deposited by RF sputtering and patterned by shadow mask in Step I. The channel layer was deposited by RF magnetron sputtering at room temperature using a 3 inch diameter InGaZnO_4 target. For the deposition of the a-IGZO film, pre-sputter was executed at the powers of 30 W and 70W in the pressure of 5×10^{-2} torr for 250 seconds. The film was deposited using a rf-sputtering system at room temperature with a power of 100W, a working pressure of 5×10^{-3} Torr, and an O_2/Ar flow rate of 0/30. The thickness of the a-IGZO channel layer was about 35nm.

4. Deposition of the Source/Drain electrode

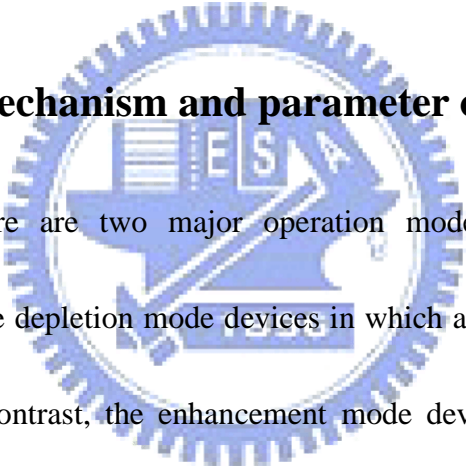
In Step II, the metal material of Ti was used as the source/drain electrodes on the a-IGZO TFTs. The thickness of the Ti electrode pad is 120nm and the S/D pattern is defined by shadow mask. As shown in Fig. 2.2, the S/D contacts were treated by the Nd:Yag laser to reduce the contact resistance before the deposition of Ti and patterned

by shadow mask..

2-1.2 Laser annealing and contact treating condition

The laser we used here were Nd:YAG solid state laser, in order to get the channel layer from conduction to insulation, we change the lens position to vary the laser power, the detail list in Table 2.1 and system show in Fig. 2.3. To move the pinhole position to control the LASER power applied on devices.

2-2 Operation mechanism and parameter of transistor



In the TFTs, there are two major operation modes, depletion mode and enhancement mode. The depletion mode devices in which a channel already exists at zero gate voltage. In contrast, the enhancement mode devices in which a channel exists at the gate voltage applied. The ideal device for TFTs were enhancement mode, it have very low leakage current at zero gate voltage. However the a-IGZO is an n-channel material and we need to apply the positive voltage to form a channel path. The delocalized electrons that are accumulated near the active layer/insulator interface when a positive voltage is applied to the gate contact provide a path for current conduction, which is denoted as the channel. As a positive voltage is applied to the drain electrode of the TFTs, these delocalized electrons in the accumulation layer are

extracted from the channel, giving rise to drain current path through the TFTs. The later section we will report the definition of linear region and saturation region and their current function.

2-2.1 Linear region

When the small positive drain voltages, i.e., voltages smaller than the gate voltage minus the threshold voltage, $V_{DS} < V_{GS} - V_{TH}$, the drain current conduction can be modeled as a linear relationship as is given by

$$I_D = \frac{1}{2} \mu C_{ox} \frac{W}{L} [2(V_{GS} - V_{TH})V_{DS} - V_{DS}^2] \quad (2-1)$$

where the threshold voltage (V_{TH}) is the voltage at which the intercept point of the square-root of drain current versus voltage when the device operate in saturation mode, C_{ox} is the oxide capacitance, μ is the mobility of the electrons, W is the width of the channel, L is the length of the channel. V_{GS} and V_{DS} are the gate-to-source and drain-to-source voltage, respectively.

2-2.2 Saturation region

As the drain voltage reaches the pinch-off voltage, i.e., the voltage at the channel near the drain is depleted of carriers, $V_{DS} \geq V_{GS} - V_{ON}$, the drain current saturates, thus the current independent of the drain voltage and is given by

$$I_D = \frac{1}{2} \mu C_{ox} \frac{W}{L} (V_{GS} - V_{TH})^2 \quad (2-2)$$

2-2.3 Mobility

Mobility is a measurement of how fast carriers can move in material. A higher magnitude of mobility allows for a faster switching time, i.e., the time it takes for the device switching from the off state to on state. A larger mobility value means that the device can conduct more current. Generally, mobility can be extracted from the transconductance maximum g_m in the linear region:

$$g_m = \left[\frac{\partial I_D}{\partial V_G} \right]_{V_D = \text{const}} = \frac{W C_{ox}}{L} \mu_{\text{linear}} V_D \quad (2-3)$$

The saturation mobility is another commonly used type of mobility. It is extracted from an ID-VG curve when the device is biased in saturation. [39] The saturation mobility is calculated as

$$\mu_{\text{sat}} = \left[\frac{2m^2}{\frac{W}{L} C_{ox}} \right]_{\text{saturation}} \quad (2-4)$$

2-2.4 Threshold Voltage

Threshold voltage is related to the operation voltage and power consumptions of TFTs. We extract the threshold voltage from equation (2-5), the intercept point of the square-root of drain current versus voltage when the devices operate in saturation mode.

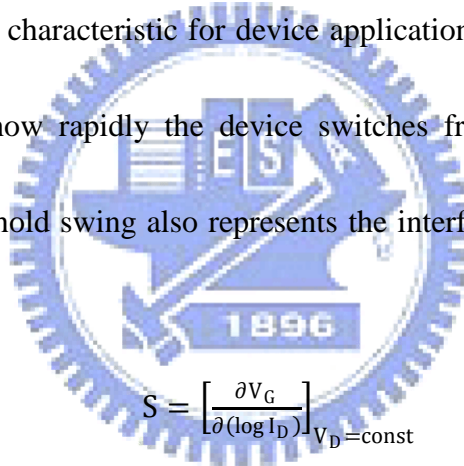
$$\sqrt{I_D} = \sqrt{\frac{W}{2L} \mu C_{OX} (V_G - V_{TH})} \quad (2-5)$$

2-2.5 I_{on}/I_{off} current ratio

The I_{on}/I_{off} (on/off) ratio represents large turn-on current and small off current. It is an indicator of how well a device will work as a switch. A large on/off current ratio means there are enough turn-on current to drive the pixel and low off current to maintain in low consumption.

2-2.6 Subthreshold swing

Another important characteristic for device application is subthreshold swing. It is a measurement of how rapidly the device switches from off state to on state. Moreover, the subthreshold swing also represents the interface quality and the defect density [40].



$$S = \left[\frac{\partial V_G}{\partial (\log I_D)} \right]_{V_D = \text{const}} \quad (2-6)$$

If we want to have a better performance TFTs, we need to lower the subthreshold swing.

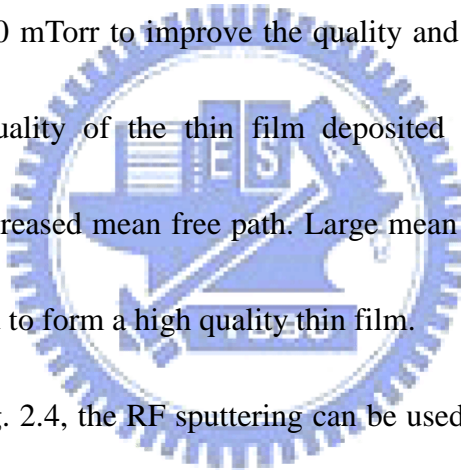
2-3 Experimental instruments

2-3.1 Sputter

1. Radio frequency sputtering

Several methods are reported to deposit a film on to a substrate. Chemical vapor deposition (CVD) and physical vapor deposition (PVD) are the most commonly used to form and deposit a film in semiconductor-based area. Sputter is one of the

deposition techniques in PVD and it can be divided into two kinds of sputtering methods: Radio frequency (RF) sputtering and direct current (DC) sputtering. RF sputtering is widely used to deposit a-IGZO in recent years. It uses a radio frequency of 13.56 MHz to generate plasma. The generated plasma creates ions to sputter the target material. The ions are accelerated towards the target by a negative DC bias on the target due to the flux of electrons. The ions hit the target with enough energy to deposit the target atoms onto the substrate. Generally, the RF sputtering is performed at the pressure of 1 - 50 mTorr to improve the quality and the deposition rate of the deposited film. The quality of the thin film deposited at the low pressure was increased due to the increased mean free path. Large mean free path helps the species to find a stable state and to form a high quality thin film.



As shown in Fig. 2.4, the RF sputtering can be used to sputter both insulating and conducting targets. The RF voltage can be coupled capacitively through the insulating target to the plasma and charge does not build up on the surface of the target.

2. Direct current sputtering

The major change from RF to direct current (DC) sputtering is the used power supply. The mechanism of the sputtering process is unchanged. Compare to RF sputtering, the DC sputtering has higher deposition rates and lower cost. In DC sputtering system, the deposition pressure is controlled to 1-100 mTorr. As shown in

Fig. 2.5, the DC voltage is applied across electrodes to create plasma and the top electrode is the source material to be deposited. The DC sputtering use secondary electrons to sustain DC plasma, which created by the ion bombardment are accelerated away from the cathode. These electrons then pass through the cathode sheathe and collide with the Ar atoms in the negative glow region, ionizing some of them and sustaining the plasma. [41] Conventional DC sputtering can be only used to sputter the conductive targets. Ar accumulates on the $-V$ target, decreases the voltage less than to sustain the glow discharge and the plasma would shut down.

2-3.2 Electron beam evaporation

Electron beam evaporation (E-beam) is used E-beam to deposit titanium (Ti) as the electrodes in this thesis. A beam of electrons is typically with energy about ~ 10 keV and current up to several amperes. The metal was heated to the evaporation temperature by the electron beam. In the evaporation process, the outer portion of the charge was not melted to minimize the film contamination from the trace amount of impurities inside the graphite or silicon carbide crucible. [41]

2-3.3 Nd:YAG LASER

The Nd:YAG LASER is one of the solid state laser, neodymium-doped yttrium aluminum garnet (Nd:YAG, more precisely Nd^{3+} :YAG). Nd:YAG is a four-level gain

medium, offering substantial laser gain even for moderate excitation levels and pump intensities. The gain bandwidth is relatively small, but this allows for a high gain efficiency and thus low threshold pump power. The most common Nd:YAG emission wavelength is 1064 nm. Starting with that wavelength, outputs at 532, 355 and 266 nm can be generated by frequency doubling, frequency tripling and frequency quadrupling, respectively. [42] We employed here is frequency quadrupling to have the wavelength of 266nm. Because the energy source of laser has high photon energy of 4.66 eV that larger than the optical bandgap of a-IGZO (3.2eV). It could be absorb by a-IGZO film and is possible to employ Nd:YAG laser as an annealing source. The pulse duration is approximately 4ns and the energy density of single pulse is 10.7mJ/cm². During annealing process, the pulses were shot in sequence with 10Hz frequency and swept the TFTs on substrate. Laser duration of one TFT is about 1 second.

2-3.4 Ultraviolet (UV)

Another annealing method was based on ultraviolet (UV) lamp. The employed UV lamp is xenon (Xe) excimer lamp. It is formed and emitted as the following mechanism: Xe atom is excited and ionized by the high energy discharged electron. Excited Xe atom and ground state Xe atoms produce Xe excimer molecules by three-body reaction. It does not interact with the weakly bound ground state, but

decays by radiation. The spectrum is dominated by second Xe excimer continuum emission band at 172nm with 14nm half bandwidth and the power density is around 50mW/cm² [43]. Because the photon energy is quite high (7.2 eV) and photon absorbing of oxygen is easy, the sample must be set in an isolated box with introducing nitrogen to expel oxygen. The high photon energy (7.2eV) is larger than band gap of metal oxide and emitted photon could be effectively absorbed by a-IGZO.

2-3.5 Four-point probe resistivity measurement

A standard way of measuring electrical resistance of a sample is by passing current through the sample and measuring the voltage drop across it and taking the ratio of the voltage to the current. However in this method the electrical resistance of the contacts is also measured along with the resistance of the sample. This can be neglected if the resistance of the sample is very high, but usually when measuring the sheet resistance of semiconductor samples, the contact resistance cannot be neglected.

A four point probe configuration is usually used to measure the sheet resistance of a semiconductor. A standard four point probe set up is shown in Fig. 2.6 below. Four identical probes are placed in a linear configuration, equally spaced, along the sample. Current is forced through the outer probes, while the voltage is measured across the inner probes. The voltage is measured using a high impedance meter, which minimizes the current flow, thereby minimizing the contact resistance to a negligible

value.



Figure of chapter 2

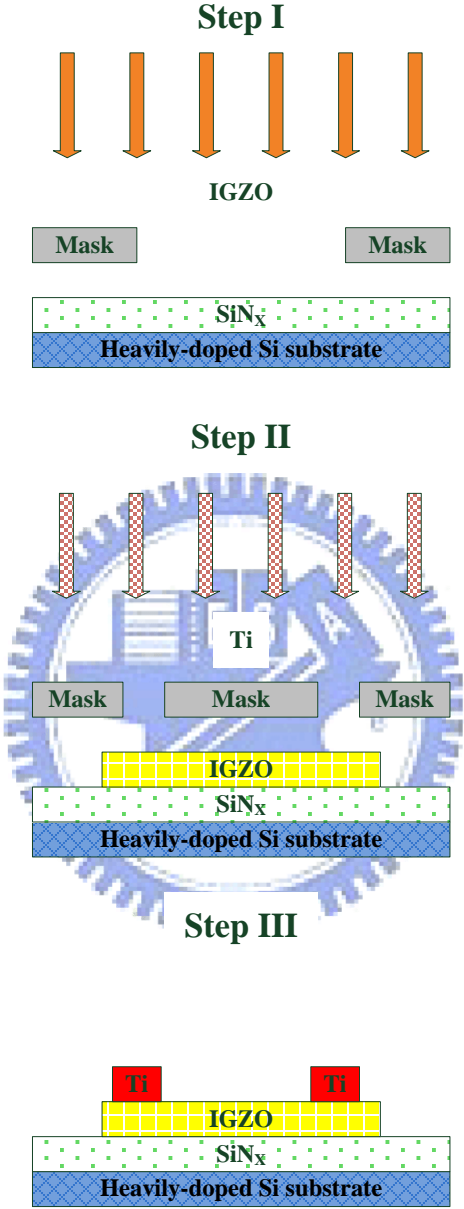


Fig. 2.1 The a-IGZO TFTs fabrication process.

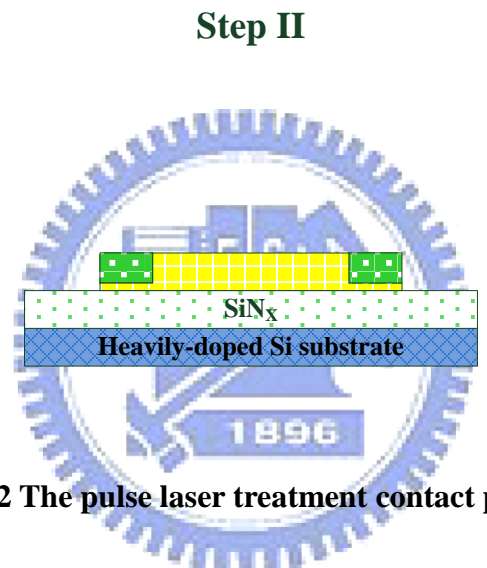
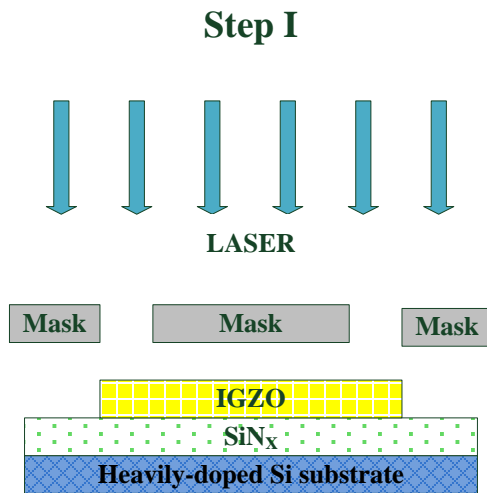


Fig. 2.2 The pulse laser treatment contact process.

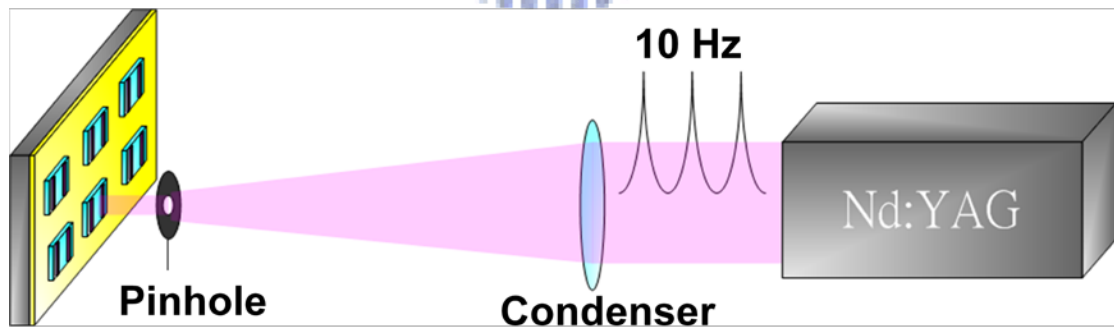


Fig. 2.3 The pulse laser annealing system.

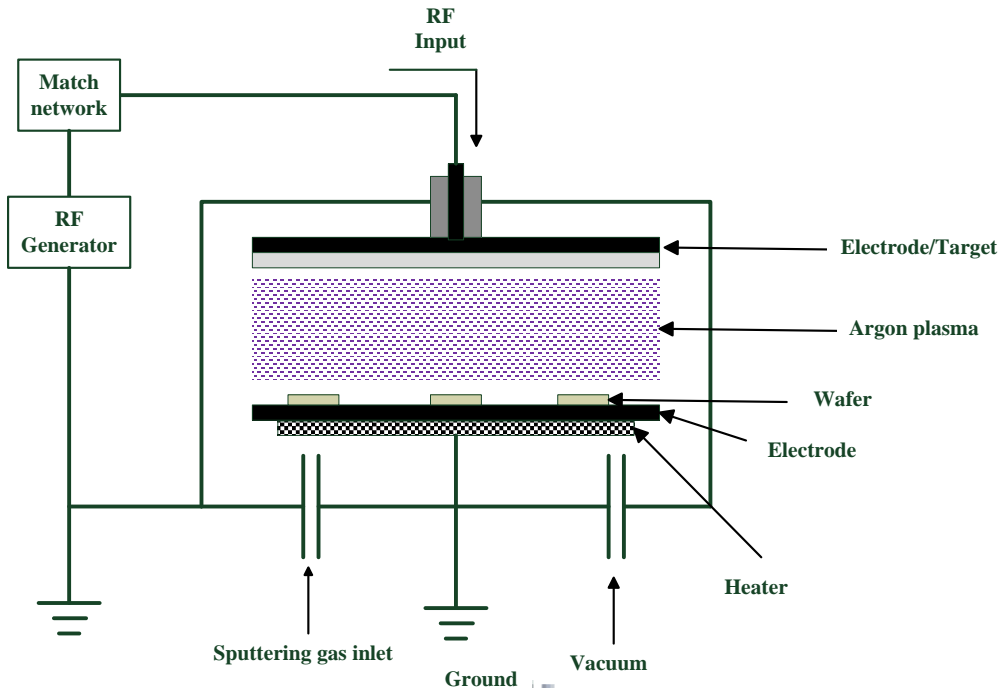


Fig. 2.4 The RF-power sputtering deposition system.

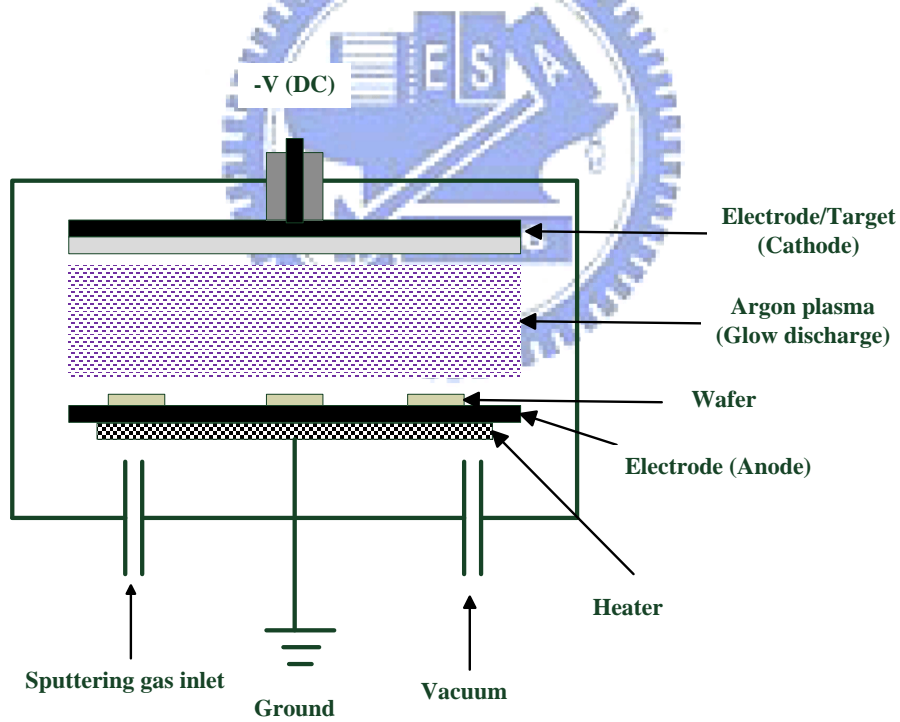


Fig. 2.5 The DC-powered sputter deposition system.

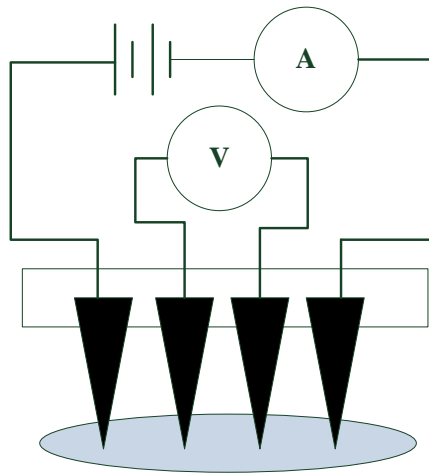


Fig. 2.6 Four-point probe.

Position	Radius (cm)	Area (cm²)	Energy Density (mJ/cm²)
+5	0.045	0.006	267.36
+4	0.060	0.011	150.39
+3	0.075	0.018	96.25
+2	0.090	0.025	66.84
+1	0.105	0.035	49.11
0	0.120	0.045	37.60
-1	0.135	0.057	29.71
-2	0.150	0.071	24.06
-3	0.165	0.085	19.89
-4	0.180	0.102	16.71
-5	0.195	0.119	14.24
-6	0.210	0.138	12.28
-7	0.225	0.159	10.69
-7.5	0.233	0.170	10.02

Table 2.1 Laser intensity conditions.

Chapter 3

Results and Discussions

3-1 Instability of as-fabricated a-IGZO TFTs

Low temperature fabricated transistor ($<150^{\circ}\text{C}$) is one of promising destinations of metal oxide that attract the most attention. Nevertheless, when the deposition process of metal oxide channel layer is executed at low temperature, the transistors are quite unstable. [12,13] Figure 3.1 shows the sequent transfer characteristics (I_D - V_G curve) of a-IGZO TFTs that include eight times forward sweeping measurements (V_G ranging from -15V to 20V) and eight times backward sweeping measurements (V_G ranging from 20V to -15V) before post-annealing. As shown in Fig. 3.1, the threshold voltage of transfer curve shift to positive direction with sequent measurements. The result mentioned above demonstrate that the as-fabricated a-IGZO TFTs without post-annealing treatment are unstable. Figures 3.2, 3.3, 3.4 and 3.5 shows the evolutions of threshold voltage (V), field effective mobility (cm^2/Vs), subthreshold swing (V/dec.) and drain current at $V_D=20\text{V}$ extracted from the data in Fig. 3.1, respectively. As shown in Fig. 3.2 and 3.3, the threshold voltage and mobility increased with sequent I_D - V_G curve measurement (Threshold voltage ranging from 3.3V to 15.9V, field effective mobility ranging from 0.96 to 5.09 cm^2/Vs). Backward sweeping has higher ability to shift the I_D - V_G curve because the saturated threshold

during sequent forward sweeping was varied in depth. The threshold voltage shift during sequent operation which maybe caused by an electron trapping center that also plays a mobile carrier scattering center. Therefore, if the electron trapping centers occupied by mobile electrons, the threshold voltage and mobility will both increase at the same time. The trapped mobile electrons will not be entirely released before the next I_D - V_G measurement, therefore the larger threshold voltage will be observed during the next measurement. The increase of occupied trapping states means the decrease of scattering probability that lead to increase of mobility. The defect that induce serious threshold voltage shift maybe caused by the disorder structure of room temperature deposited a-IGZO film. In this study, we assume that the mobile electrons were trapped on channel/dielectric interface after I_D - V_G curve measurement that reduce the quantity of mobile carries at one gate voltage. On the other hand, lager positive gate voltage is needed to turn the IGZO TFT for the following I_D - V_G measurement. [44] Backward sweeping could induce more threshold voltage shift after the threshold voltage achieved saturation during sequent forward sweeping measurements that could be explained by the suddenly applied large positive V_G in the beginning. As shown in Fig. 3.4, the subthreshold swing is fluctuant during sequent I_D - V_G curve measurements, backward sweeping especially. Figure 3.5 presents the evolution of drain current at gate voltage of 20 V with sequent

measurements. Reducing drain current at one gate voltage is quit easy for un-annealed TFTs caused by the serious instability. The current level decreased one order after just few times sequent measurements (varying from 10^{-5} to 10^{-6}). The as-fabricated a-IGZO TFTs never attain stable state because the shifted threshold will recover after an idle period as shown in Fig. 3.6. We executed seven times sequent I_D - V_G curve measurement twice with an idle interval of half hour. The result shows that the transfer curve somewhat recovered after an idle period. The experiment result mentioned above demonstrated that the as-fabricated a-IGZO TFTs are very unstable before post-annealing. We executed seven times sequent transfer curve measurement because the threshold voltage will achieve saturation within seven times. Therefore the deviation of seven sequent I_D - V_G curves could effectively reflect the instability.

3-2 Effect of Post-annealing

In this study, we demonstrate that appropriate post-annealing could make a-IGZO TFTs adequately stable. The stability of a-IGZO TFTs were graded by the threshold voltage shift during sequent I_D - V_G curve measurement.

Here, we defined the parameter, ΔV_{TH} , to reflect the instability of a-IGZO TFTs.

$$\Delta V_{TH} \equiv V_{TH\ 7th} - V_{TH\ 1st} \quad (3-1)$$

ΔV_{TH} is the difference of threshold voltages of the first and seventh transfer curve. In this study, we roughly judged the adequate annealing by threshold voltage of less than

0.5 V. Smaller ΔV_{TH} means more stable characteristic of IGZO TFT.

In this section, we compare five a-IGZO TFTs with various annealing conditions. The various annealing conditions are un-annealing, furnace annealing at 300°C in nitrogen atmosphere, furnace annealing at 350°C in nitrogen atmosphere (commonly used in papers [45-49]), pulse laser annealing and UV lamp annealing. Figures 3.7, 3.8, 3.9, 3.10 and 3.11 show the seven times sequent transfer characteristics of five various annealing respectively. As shown in Fig. 3.7, un-annealed a-IGZO TFT was quite unstable ($\Delta V_{TH}=10.8V$). The as-deposited a-IGZO TFT may has a lot of defect states caused by disorder structure on the channel/dielectric interface, and the defect states are trapping centers for mobile electrons. The applied positive gate voltage will induce the trapping process. The reduction of mobile electron at one gate voltage results in lower drain current. Therefore a larger positive voltage is required to turn on the transistor [44]. The threshold voltage will achieve saturation after some times sequent I_D-V_G curve measurement. In fact, the saturated transfer curve could shift again by applying higher gate bias. The measurement result demonstrate that the as-deposited a-IGZO TFT is quite unstable.

Then two thermal annealing were compared, Fig. 3.8 and 3.9 show the effect of furnace annealing at different temperature in nitrogen atmosphere. In Fig. 3.8, the annealing condition involves temperature of 300 °C, nitrogen flow rate of 10L/min

and period of one hour. Although the criteria like field effective mobility ($9.54 \text{ cm}^2/\text{Vs}$), threshold voltage (2.8V) and subthreshold swing (0.1 V/dec.) as shown in Table 3.1 are satisfied, the stability was still inadequate ($\Delta V_{\text{TH}}=1.6\text{V}$). Therefore, furnace annealing at $300 \text{ }^\circ\text{C}$ is not an appropriate condition. In chapter 1, we have concluded that the temperature of more than $300 \text{ }^\circ\text{C}$ was required to have stable a-IGZO TFT. To improve the stability, a higher temperature of $350 \text{ }^\circ\text{C}$ was used to get more stable a-IGZO TFTs. As shown in Fig. 3.9, The threshold voltage shift of $350 \text{ }^\circ\text{C}$ annealed IGZO TFT decreased in depth ($\Delta V_{\text{TH}}=0.5\text{V}$) as compared with the one treated with $300 \text{ }^\circ\text{C}$ thermal annealing. The temperature of $350 \text{ }^\circ\text{C}$ was used generally in published papers [45-49]. The parameters of a $350 \text{ }^\circ\text{C}$ furnace annealed a-IGZO TFT is listed in table 3.1. All parameters presented in this study were extracted from the seventh $I_{\text{D}}-V_{\text{G}}$ curve in sequent measurement to make objectively comparison.

In Figs. 3.10 and 3.11, the effect of pulse laser and UV lamp annealing was presented respectively. Sequentially probed transfer curves of pulse laser and UV lamp annealing present adequate repeatability within seven times measurements ($\Delta V_{\text{TH}}=0.5\text{V}$ for pulse laser and $\Delta V_{\text{TH}}=0 \text{ V}$ for UV lamp). Other parameters such as mobility, subthreshold swing and on/off ration are accepted listed in Table 3.1. The stability of light annealed IGZO TFTs are comparable to the one of $350 \text{ }^\circ\text{C}$ thermal annealing. Therefore, pulse laser and UV lamp annealing are valid post-annealing

methods. As shown in Fig. 3.12(a), the estimated penetration depth of light at 266nm wavelength in a-IGZO film was about 95 nm. At a wavelength of 266nm, the absorptance was roughly 30%, which shows that the pulse laser light was efficiently and uniformly absorbed throughout the entire a-IGZO film thickness, shown in Fig. 3.12(b). The pulse laser with wavelength at 266 nm could provide enough energy to realign the atoms in a-IGZO film and make the structure more order. The laser annealing process could keep low temperature for substrate. The UV lamp at wavelength of 172nm is also a feasible light source for annealing. Because the photon energy of 7.2 eV is larger than the bandgap of a-IGZO film. Pulse laser annealing is relatively quick process for single TFT as compared with furnace annealing. The laser exposure time on one single TFT is just few seconds. The furnace annealing requires the temperature of more than 300 °C and a period of one hour to get comparably stable device. It can be extrapolated that the low temperature fabrication process will be demanded for future industry and the laser or UV lamp annealing is a potential instrument.

3-3 I_D - V_D Diagram

Output characteristic (I_D - V_D) diagram is an important tool to present the characteristics of a transistor. Figure 3.13 show four I_D - V_D diagrams for four various annealing methods by cyclic sweeping measurement with V_D ranging from 0V to 20V.

Figure 3.13 (a) present the I_D - V_D diagram of as-fabricated a-IGZO TFT. Figures 3.13 (b), (c) and (d) belongs to the a-IGZO TFT treated with furnace annealing at 350°C in nitrogen atmosphere, pulse laser annealing and UV lamp annealing, respectively. The I_D - V_D curves probed by cyclic sweeping could reflect both the adjustability of current and stability. The stability could be graded by the deviation between two cyclic curves. As shown in Fig. 3.13 (a), the saturation current was relatively low as compared with the one of 350 °C furnace annealed IGZO TFT that could be explained by large threshold voltage ($V_{TH}=11.1V$) attained after sequent measurement. In Fig. 3.13 (b), 3.13 (c) and 3.13 (d), the curve slop in linear region is relatively slow maybe caused by non-negligible contact resistance. Although the threshold voltages of pulse laser and UV lamp annealed a-IGZO TFTs are small ($<0.3V$) and stable, the saturation currents in Figs. 3.13(c) and 3.13(d) are still relatively small as compared with the one in Fig. 3.13(b). That could be explained by the smaller field effective mobility and un-annealed contact. Because the metal electrode of source/drain contact could shadow the irradiation during annealing process, the region under electrode was un-illuminated that may cause non-negligible contact resistance. In fact, a-IGZO TFTs with light annealing include both pulse laser and UV lamp has degraded mobility compared with as-fabricated a-IGZO TFTs although the stability was improved. The mechanism of light annealing is underdeveloped.

3-4 Laser intensity dependence on a-IGZO TFTs during

Annealing

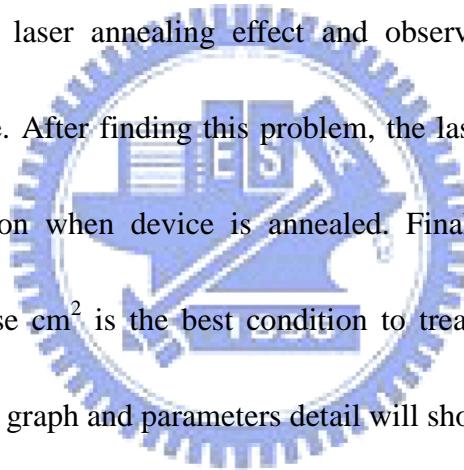
In this study, we also propose an illumination based method to treat the interface between source/drain contact and a-IGZO layer. The illumination treated a-IGZO film will possess high conductivity. Recently, several published papers reported the study of contact treatment to reduce the contact resistance [44, 13-16] like plasma treatment and RIE. This study employed a pulse laser (Nd:YAG, 266nm) to treat the contact area on a-IGZO film that could define the S/D contact directly without metal electrode or modify the interface between a-IGZO and metal electrode. Ahn et al. [50] reported that the laser irradiation with the high photon energy caused the thermal decomposition of II-VI or III-V group semiconductor. The relatively light atoms which could form gas phase will easily separate with metallic atoms due to the higher volatility than the one of metallic atoms. For example, the escaped oxygen in ZnO [51] and the escaped nitrogen in GaN [52]. Therefore, it is reasonable to assume that the oxygen component near the a-IGZO film surface was preferentially dissociated from a-IGZO film by the laser irradiation.

The employed Nd:YAG laser is a energy source with high photon energy of 4.16 eV that larger than the optical bandgap of a-IGZO (3.2eV). The laser illumination not only could stabilize the IGZO TFTs but also could vary the composition of a-IGZO

film. By our experiment result that will be discussed in detail later, laser is a feasible tool to execute contact treatment. Although pulse laser is a valid annealing method that mentioned before, the effective range of energy density (mJ/pulse cm^2) is narrow. The transfer curves with various energy densities are shown in Fig. 3.14 and the extracted parameters were listed in Table 3.2. There are three used energy densities close to the feasible annealing (10.96, 12.28 and 14.24 mJ/pulse cm^2). Energy intensity 10.96 mJ/pulse cm^2 was referred to the best among the discussed values. The energy densities exceed the feasible range between 16.71 to 267.36 mJ/pulse cm^2 are useless. Because too low energy density could not make a-IGZO TFTs adequately stable and too high energy density will make a-IGZO layer excessively conductive. The energies that could make IGZO conductive may be appropriate choices for S/D contact treatment. Base on the experiment result above, we employed 4-point probe to measure the sheet resistance as shown in Fig. 3.15. The sheet resistance at a laser energy density of 24.06 mJ/cm^2 was roughly 3 orders of magnitude less than that for an un-irradiated film. Although the higher energy seems better for contact treatment, excessively high energy density more than 100 mJ/pulse cm^2 will injury the dielectric layer and lead to serious current leakage.

Besides, when annealing applies after laser treatment and the content of the oxygen deficiency is almost to the level of the as-deposited device. This result led to

an increase in the S/D sheet resistance and degradation of TFTs performance [45]. The annealing process comes firstly could eliminate this problem, but it will become more difficult to make the film conductive. We make an assumption which the device after annealing the atoms arrangement turned into ordered and the conduction parameter for laser treatment is not like before. The annealing condition we used was furnace annealing 400°C 1hr with oxygen (O₂) flow rate 120 sccm at pressure 0.3 torr. The reason why used the furnace as this experiment process not the laser is that we wanted to get rid of the first laser annealing effect and observe the pure laser contact treatment on the device. After finding this problem, the laser power increase to find the conduction condition when device is annealed. Finally, we find out that the intensity 96.25 mJ/Pulse cm² is the best condition to treat the film after annealed, shown in Fig. 3.16. The graph and parameters detail will show in later section.



3-5 UV intensity dependence on a-IGZO TFTs during

Annealing

The effect of illumination time of UV lamp is also discussed in this study. Figure 3.17 presents the transfer characteristics with various UV illumination time and the parameters extracted from the data in Fig. 3.17 are listed in Table 3.3. The 30 minutes is the best illumination period among the discussed values ($\Delta V_{TH}=0V$, $\mu=3.49$ cm²/Vs, $V_{TH}=0.2V$, S.S.=0.71 V/dec. and on/off= 2.5×10^6). The a-IGZO film becomes

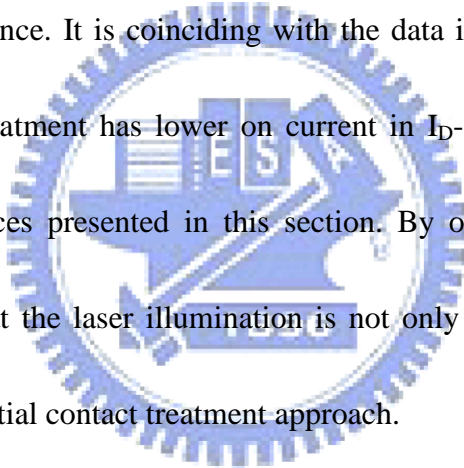
excessively conductive as the illumination time more than 30 minutes. On the contrary, the a-IGZO channel will not be annealed adequately when the illumination time less than 30 minutes. In Fig. 3.18, shows the sheet resistance with different UV illuminate time. The sheet resistance after 3 hours illumination decreases about 3 orders. The conductivity of a-IGZO channel after annealing with UV lamp could not achieve the high value that could be attained by pulse laser as shown in Fig. 3.19 even the illumination time is as long as 3.5 hours. Therefore the pulse laser is more suitable than UV lamp to define an area on a-IGZO film with high conductivity.

3-6 Result of contact pattern by laser illumination

In this study, the feasibility of contact pattern by light illumination is demonstrated. Figure 3.20 is the flow charts that present the light pattern procedure. Before light pattern process, the stack of a-IGZO/SiN_x/wafer was annealed in furnace at 400°C for 1 hour. The oxygen flow rate of 120 sccm and the furnace pressure of 0.3 torr were maintained during annealing process. There are three device structures with various contact treatment were investigated in this study. The source/drain contacts were patterned by pulse laser illumination directly of the first a-IGZO TFTs denoted by Sample (A). The second a-IGZO TFT denoted Sample (B) equipped with Ti pads on the area treated by pulse laser previously to form the source/drain contact. Ti pads serve as source/drain contacts in the third IGZO TFT which denoted by Sample (C).

Sample (C) was not subjected any laser treatment. The Ti pads of the IGZO TFTs mentioned above were deposited by e-beam evaporation. Figures 3.21 and 3.22 is the diagram of transfer characteristic (I_D - V_G) and diagram of output characteristic (I_D - V_D), respectively. The figures 3.21 and 3.22 could present the effect of laser treatment on source/drain contact. Accepted transfer curves of Sample (A), Sample (B) and Sample (C) in Fig. 3.21 demonstrate that light patterning is a feasible method and that could be applied in depth for other critic structure like self-aligned top gate TFT. Compare transfer curves of Sample (A) and Sample (C) in figure 3.21, Sample (A) ($I_D=9.06\times 10^{-5}$ A) with laser only treated source/drain contact shows larger on current than Sample (C) ($I_D=6.94\times 10^{-5}$ A) with metal electrode at $V_G=20$ V. The mobility of Sample (A) is also larger than the one of Sample (C). It could be concluded that the a-IGZO contact formed by laser treatment is more suitable than Ti electrode for electron injection. Chung et al. [53] reported that the portion of contact resistance of IGZO TFT originated from the bulk of a-IGZO is rather than the one originated from the interface between the S/D electrode and a-IGZO. The transfer curves of Sample (B) and Sample (C) were compared in figure 3.21, Sample (B) with laser treated interface between a-IGZO film and metal electrode present higher field effective mobility and on current ($\mu=9.78$ cm²/Vs, $I_D=1.44\times 10^{-4}$ A at V_G of 20V for Sample (B) ; $\mu=6.85$ cm²/Vs, $I_D=6.94\times 10^{-5}$ A at V_G of 20V for Sample (C)). The result

demonstrates that laser illumination could effectively improve the interface between the S/D contact and IGZO channel. In Fig. 3.22 compares Sample (B) and Sample (C), the laser treatment for contact could increase the saturation current twice for the a-IGZO TFT structure with metallic electrode ($I_D=1.3\times 10^{-4}$ A at V_G of 20V for Sample (A); $I_D=6.94\times 10^{-5}$ A at V_G of 20V for Sample (C)). Parameters extracted from figures, such as mobility, subthreshold swing and on/off ratio are listed in Table 3.4. The performance improvement of a-IGZO TFTs by laser treatment may be caused by reducing contact resistance. It is coinciding with the data in section 3.3, the devices without any contact treatment has lower on current in I_D - V_D diagram as compared with light treated devices presented in this section. By our experimental result, it could be concluded that the laser illumination is not only a feasible post-annealing method but also a potential contact treatment approach.

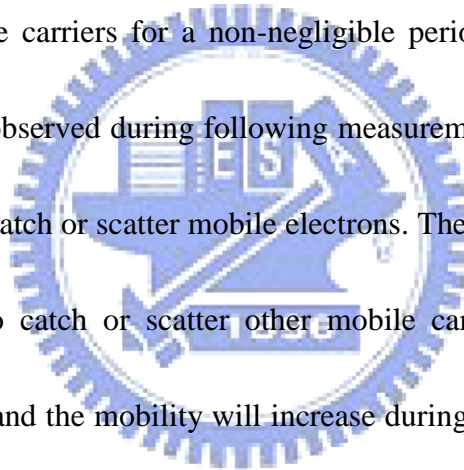


3-7 Assumption

3-7.1 Mechanism of mobile carrier trapping

The as-fabricated a-IGZO TFTs with low-temperature deposition process of IGZO channel layer was quite unstable before post-annealing. The instability may be caused by the defect originated from disorder structure or weak atomic bonding. The threshold voltage could shift substantially after just few times sequent operation. It

was observed frequently that the threshold voltage achieved to the value more than 10V during sequent I_D - V_G curve measurement with gate voltage ranging from -15V to 20V. In this study, the a-IGZO channel layers deposited by rf-sputtering without substrate heating also suffer the instability issue. The arrangement of atoms in IGZO layer deposited by rf-sputtering may be poor that caused trapping defects. Defects are also potential to form by ion bombardment of sputtering ions (e.g. Ar^+). [54] The defects locate between dielectric and a-IGZO layer are considered trapping centers that could catch mobile carriers for a non-negligible period, therefore the enlarged threshold voltage was observed during following measurement. It is assumed that the defects have ability to catch or scatter mobile electrons. The electron occupied defects will lose the ability to catch or scatter other mobile carriers, therefore threshold voltage will shift little and the mobility will increase during following transfer curves measurements. [9] The trapping mechanism was shown in Fig. 3.23. The positive gate bias could induce the electric field near interface between dielectric and channel layers. The electric field bends both bands in channel and dielectric layers that cause electron trapping near SiN_x/a -IGZO interface, as shown in Fig. 3.23(a). After remove the bias, the trapped electrons were still not released as shown in Fig. 3.23(b). During next measurement, the larger positive gate voltage is required to flat the conduction band, shown in Fig. 3.23(c). Flat band voltage is the starting point to bend the band to



turn on the transistor. Moreover, we assume that the trapping defects also play as mobile carrier scattering centers. During earlier transfer curve measurement, there are lots of un-occupied defects that will make threshold shift and lower mobility as shown in Fig. 3.24. After earlier transfer curve measurements, the defects will almost be occupied that induce higher mobility as compared with the value extracted in earlier transfer curves. This is the possible reasons why the threshold voltage and the mobility of as-fabricated a-IGZO TFTs will increase following last transfer curve measurement.

3-7.2 Physical mechanisms of channel annealing by light illumination

During post-light annealing process executed by pulse laser and UV lamp, the atoms may relax to a more stable state and/or get the enough energy to re-arrange.

The relaxed and re-arranged atoms will align more order which cause the decrease of trapping defects. Reducing trapping defects mean reducing the threshold voltage shift during device operation. Stable threshold voltage is the basic demand for application.

The same mechanism could be employed to explain the furnace annealed a-IGZO TFTs.

Figure in chapter 3

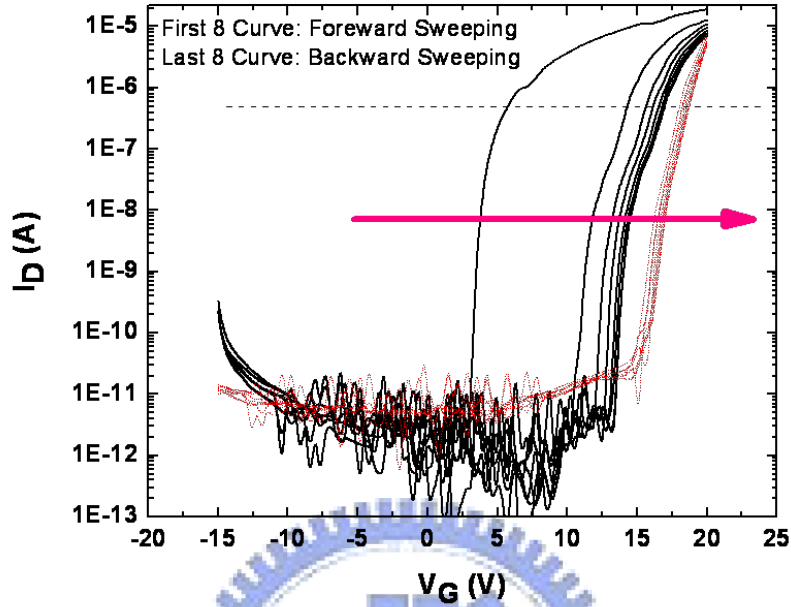


Fig. 3.1 Forward and backward eight times sweeping.

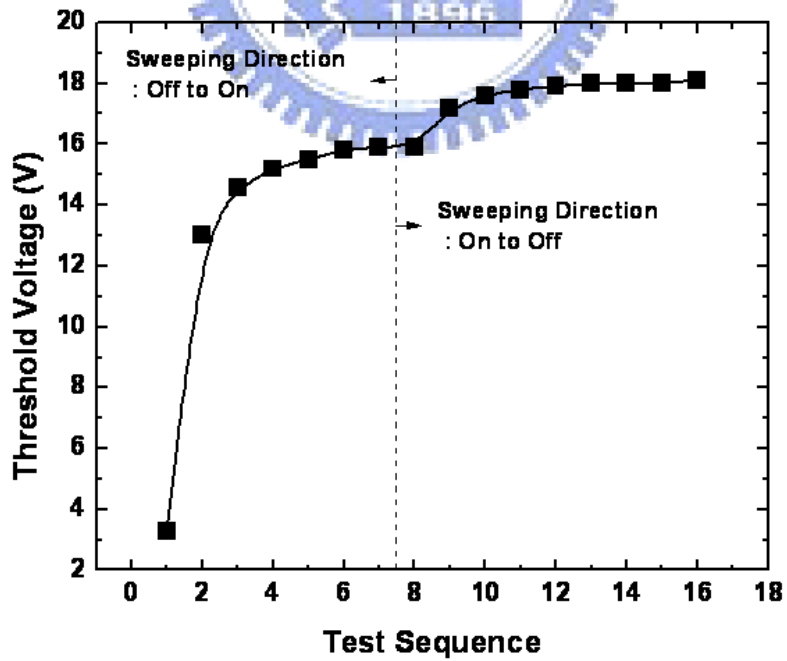


Fig. 3.2 Threshold voltage shift versus test sequence.

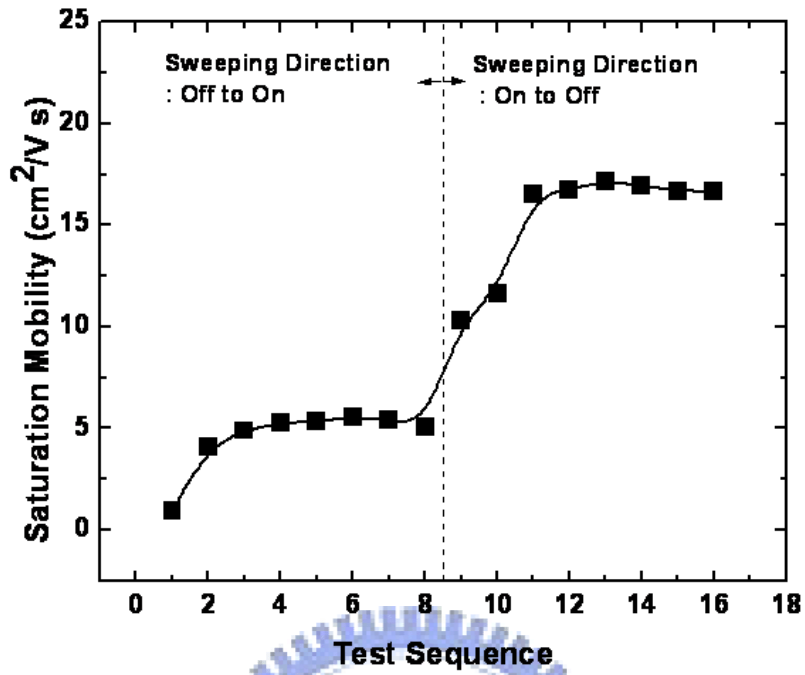


Fig. 3.3 Mobility versus test sequence.

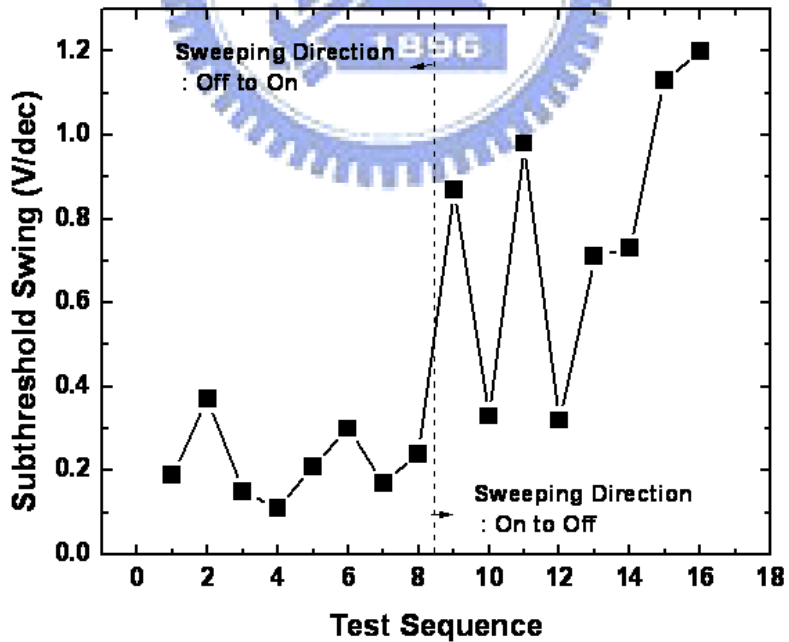


Fig. 3.4 Subthreshold swing versus test sequence.

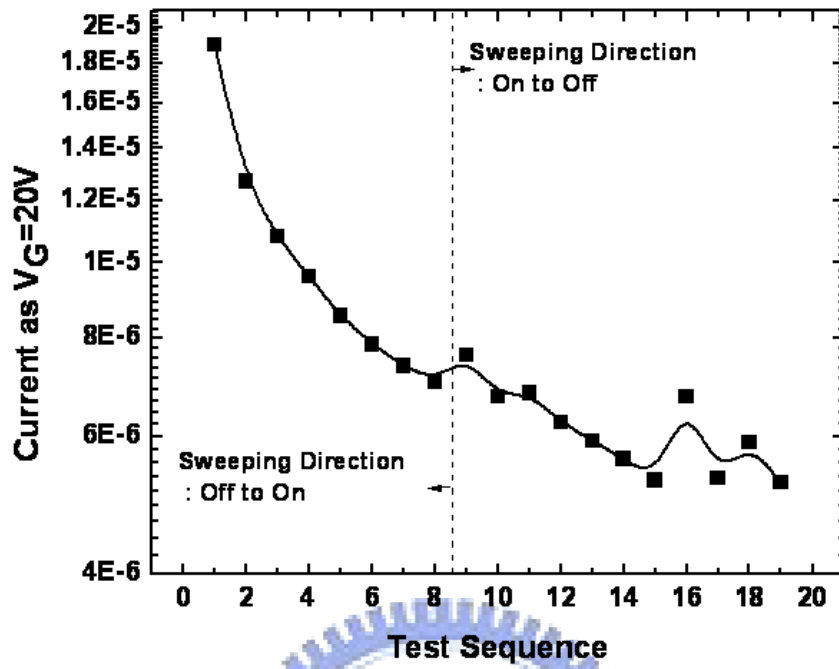
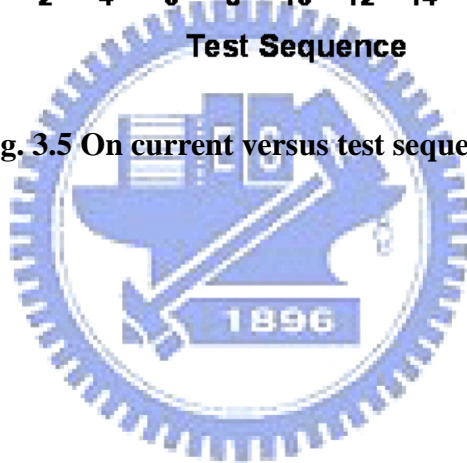


Fig. 3.5 On current versus test sequence.



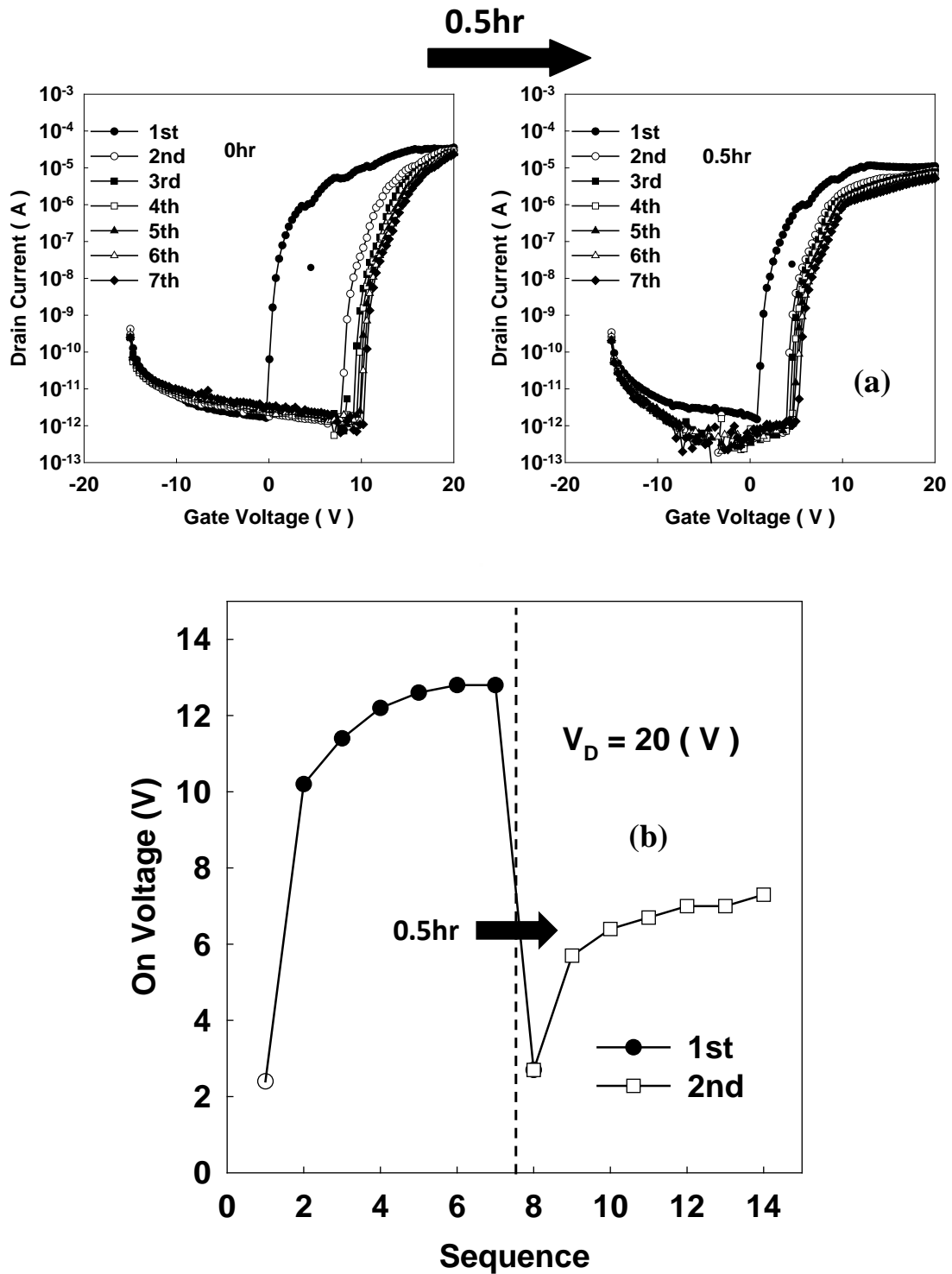


Fig. 3.6 The recovery test (a) The 7 times measurement transfer characteristic for 0min and idle 30min. (b) The on voltage shift versus measurement sequence for 0min and idle 30min.

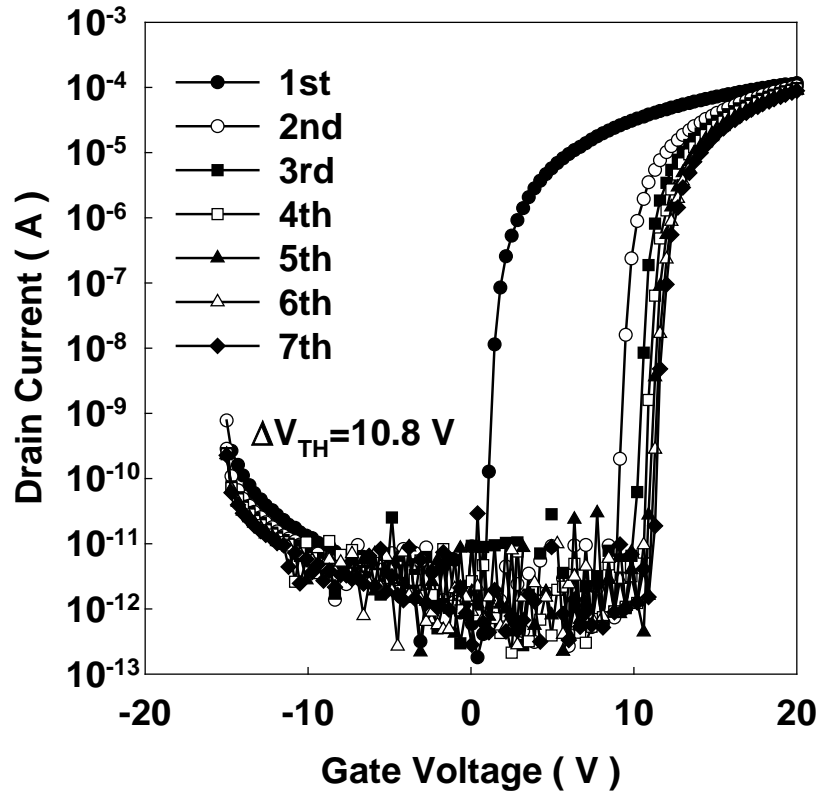


Fig. 3.7 The transfer characteristic of as-fabricated a-IGZO TFTs.

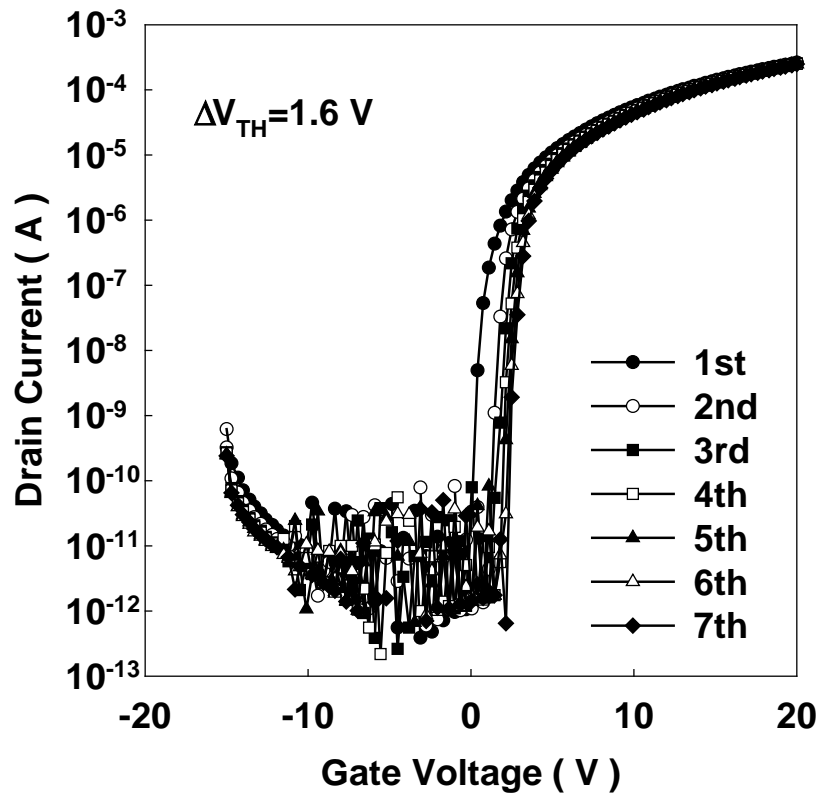


Fig. 3.8 The transfer characteristic of furnace annealed 300°C in N₂ a-IGZO TFTs.

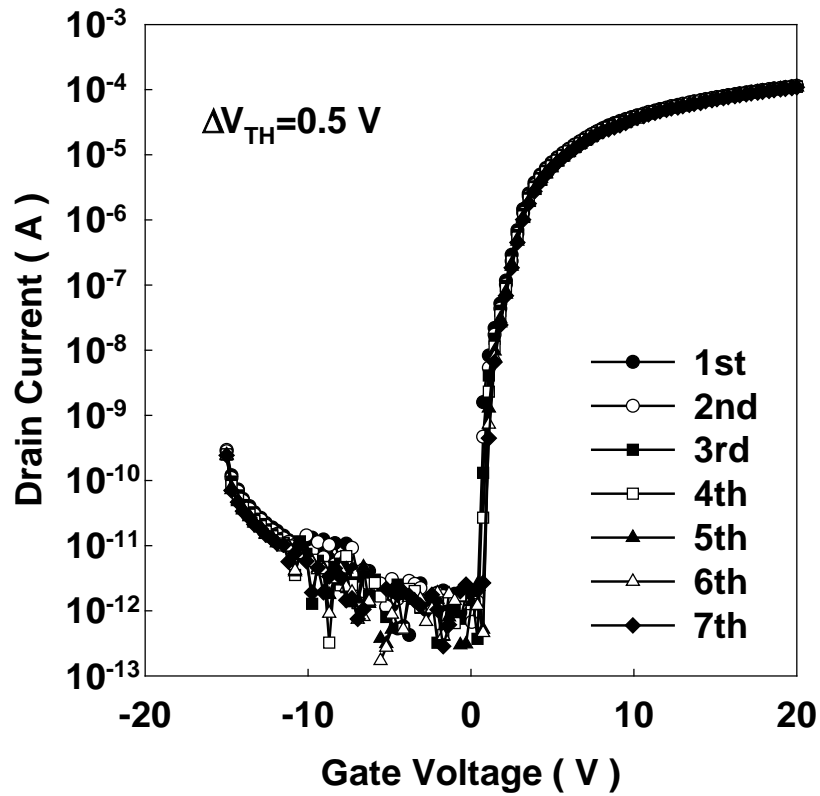


Fig. 3.9 The transfer characteristic of furnace annealed 350°C in N₂ a-IGZO TFTs.

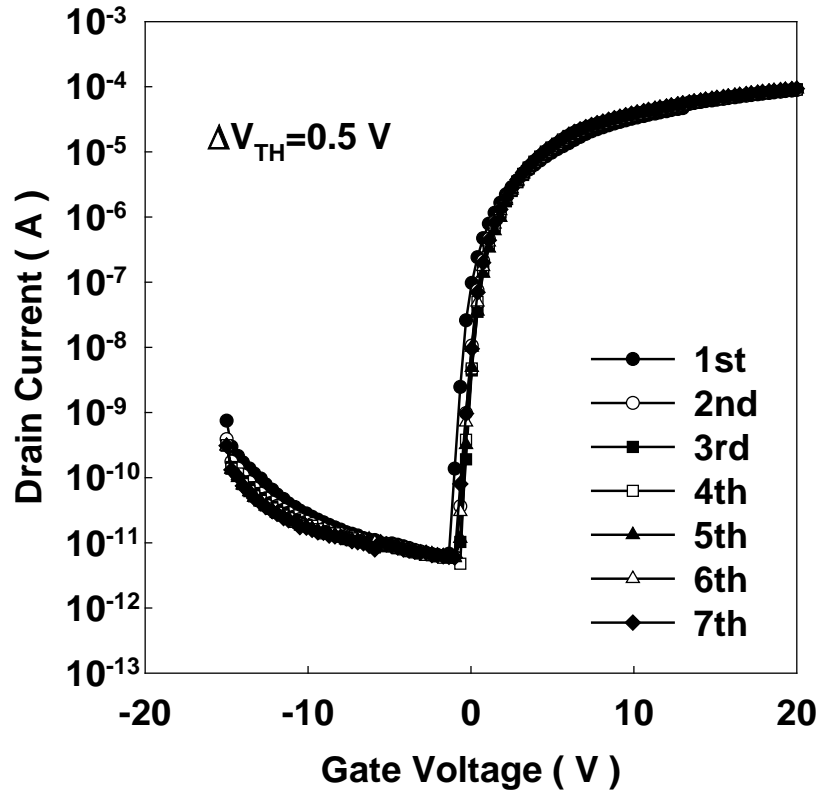


Fig. 3.10 The transfer characteristic of pulse laser annealed a-IGZO TFTs.

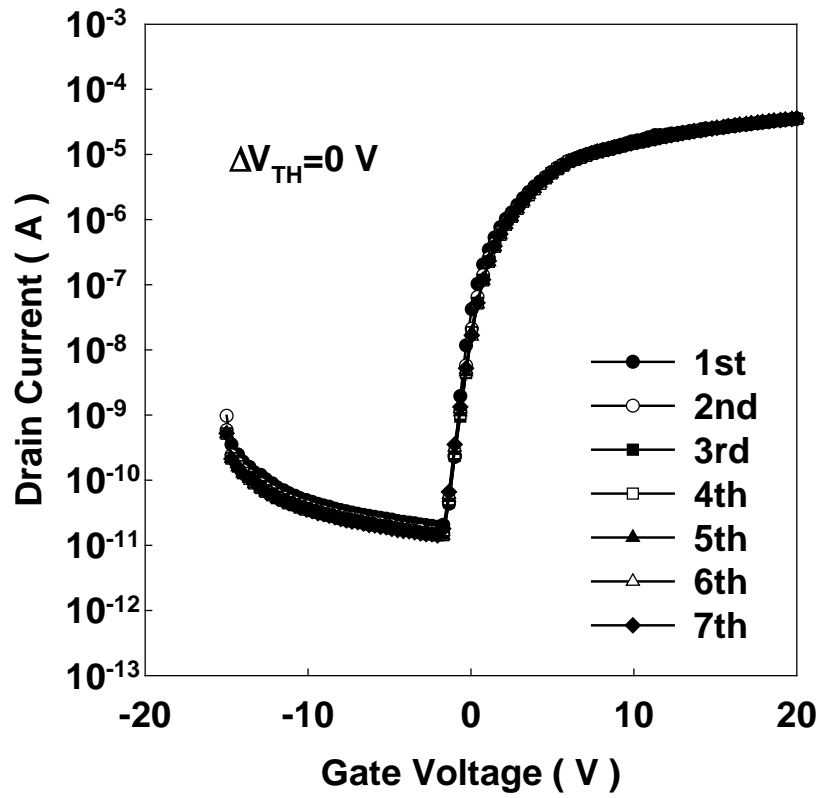


Fig. 3.11 The transfer characteristic of UV lamp annealed a-IGZO TFTs.



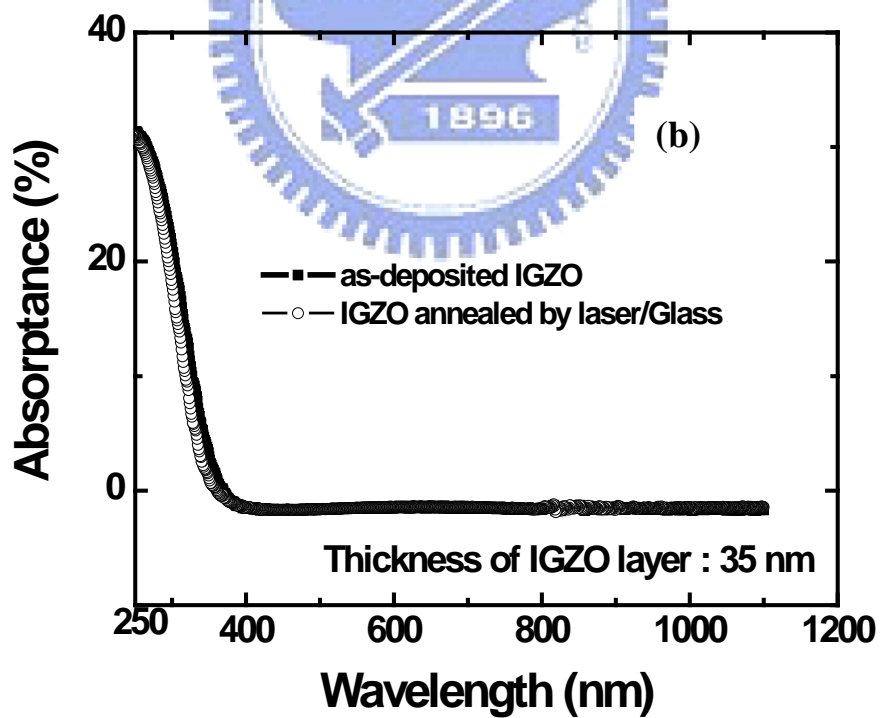
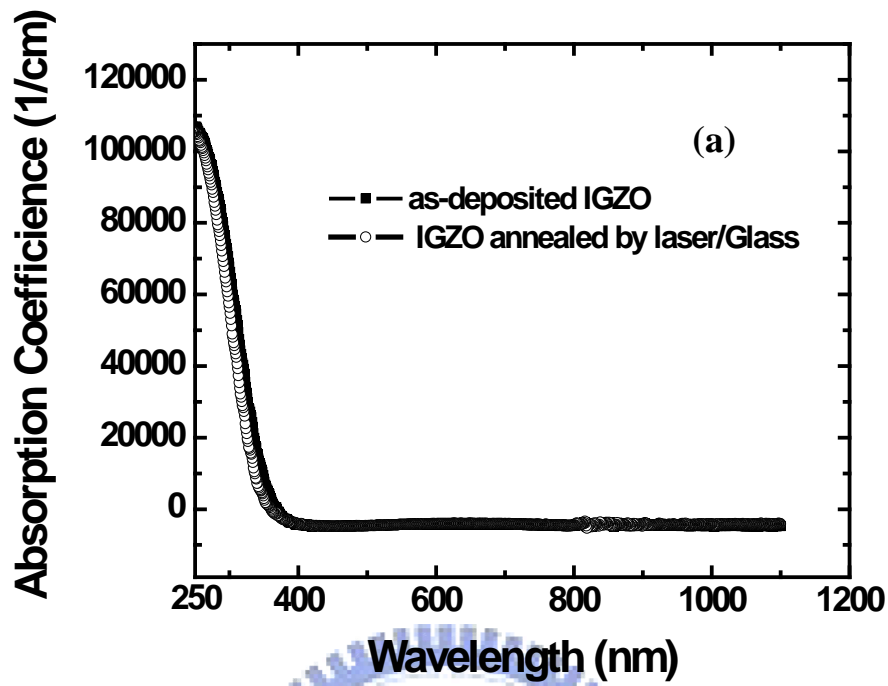


Fig. 3.12 The (a) absorption coefficient and (b) absorbance of as-deposited IGZO and IGZO annealed by laser.

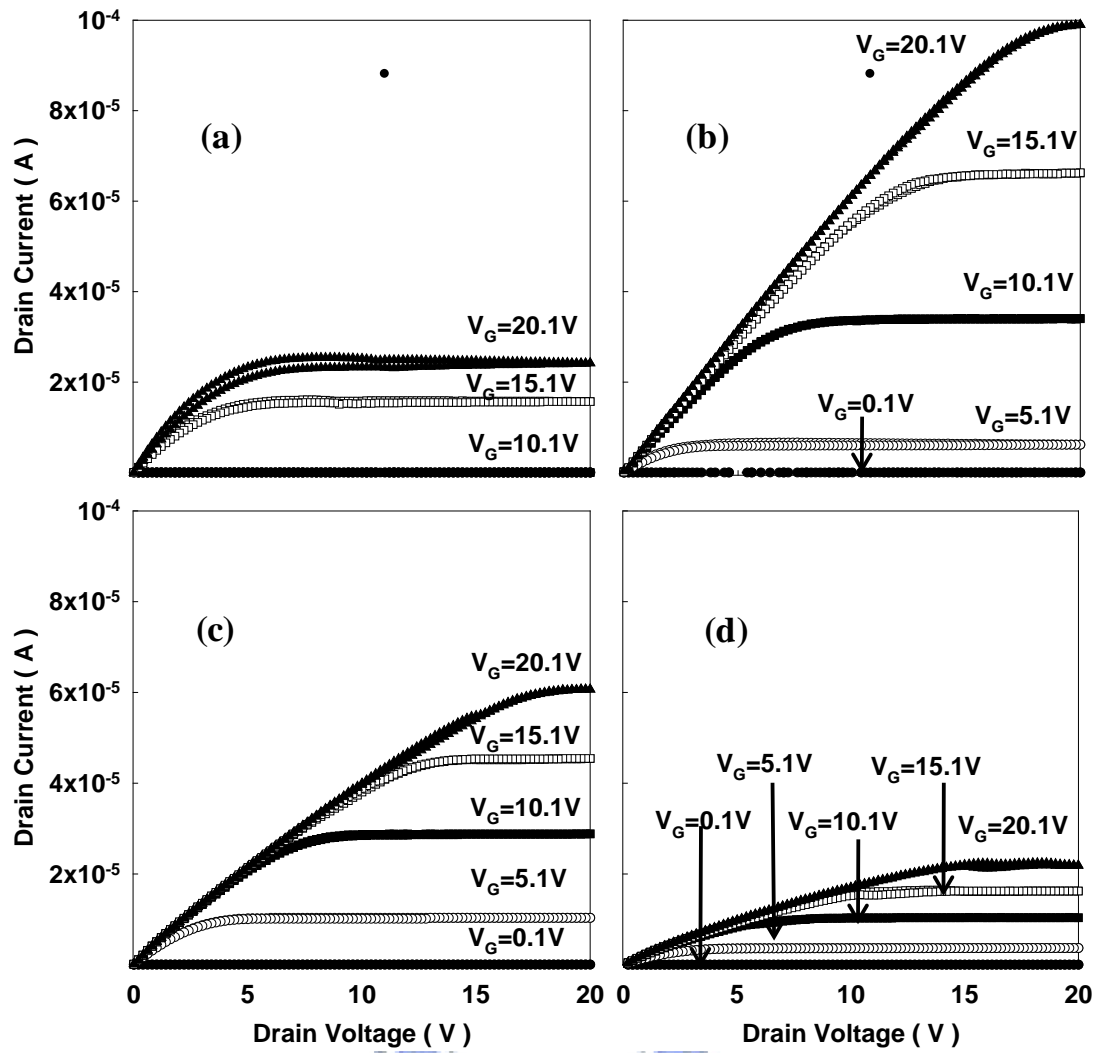


Fig. 3.13 The output characteristic diagrams for (a) as-fabricated, (b) furnace annealing 350°C in N_2 , (c) pulse laser annealing and (d) UV lamp annealing. The V_G is from 0.1 V to 20.1 V and step is 10 V.

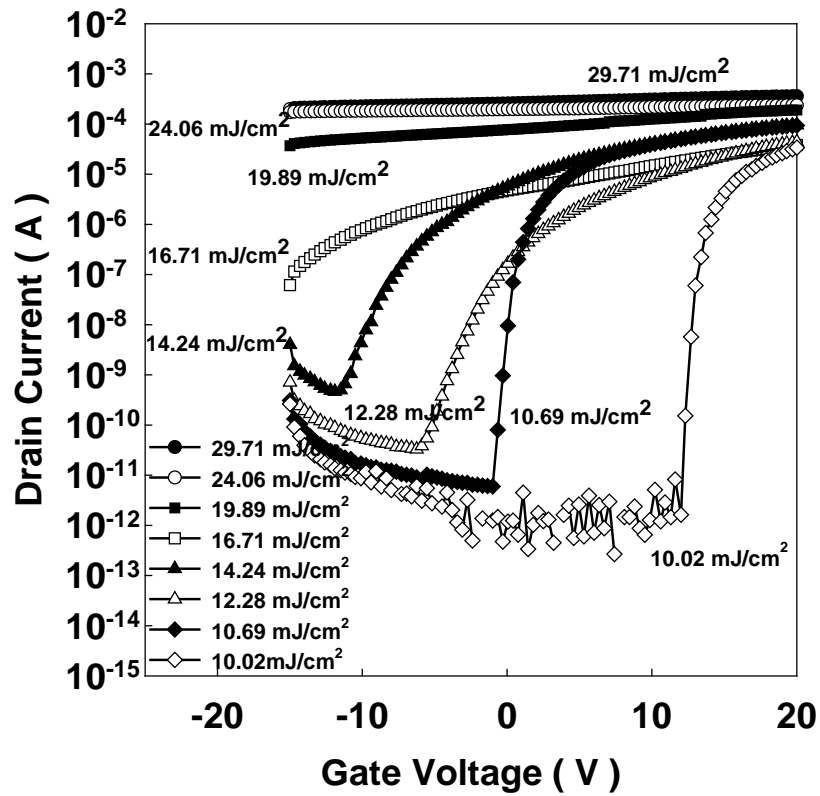


Fig. 3.14 The transfer characteristic with different pulse laser energy density treatment (10.02~29.71 mJ/cm²).

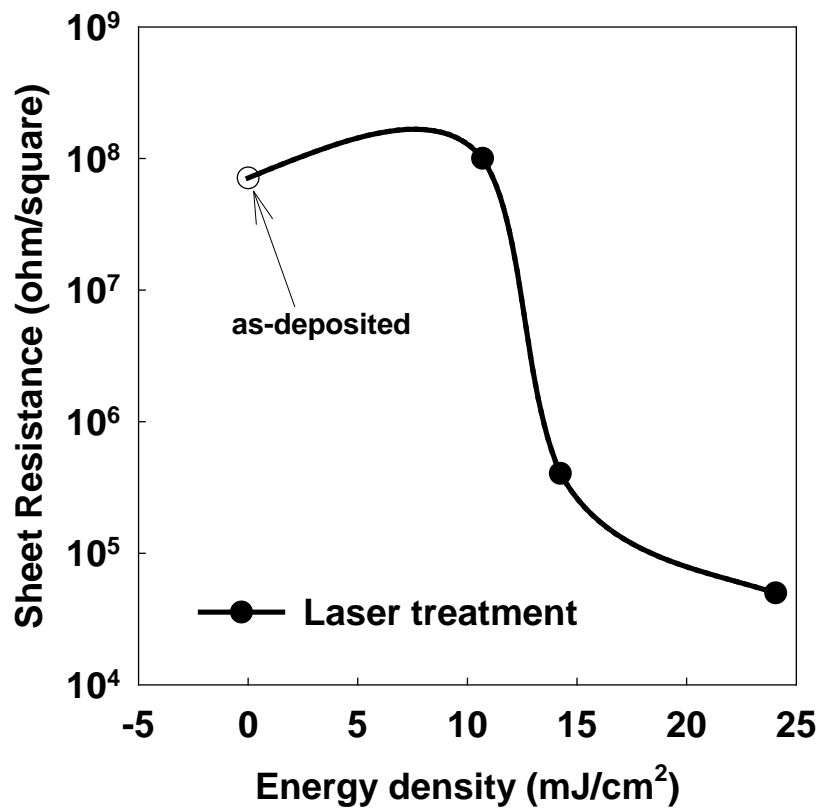


Fig. 3.15 The sheet resistance with different pulse laser energy density.

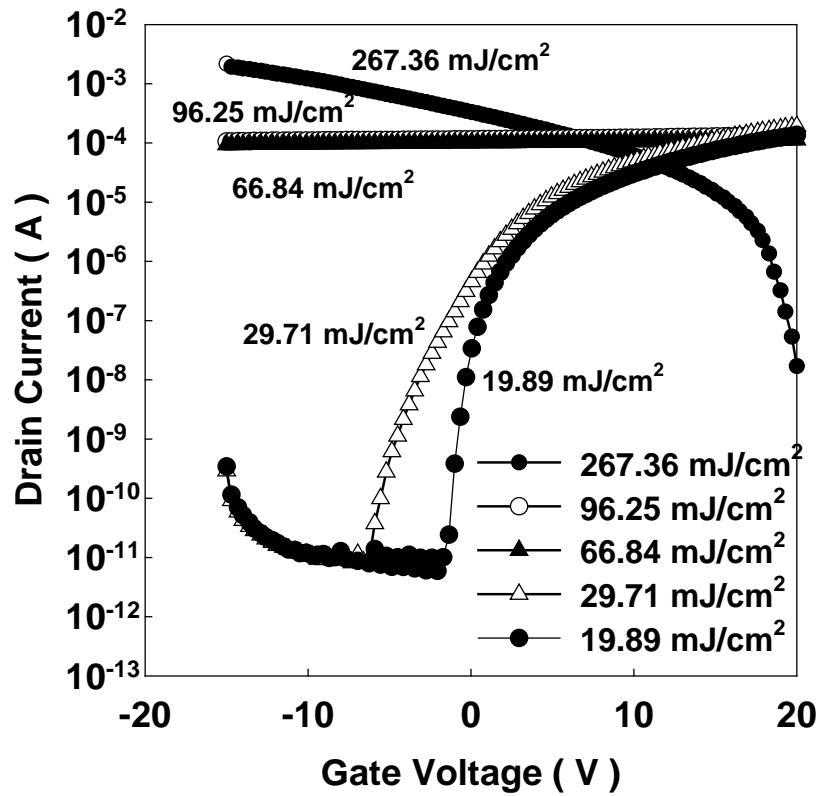


Fig. 3.16 The transfer characteristic with different pulse laser energy treatment after furnace annealing 400°C , O_2 flow 120 sccm, pressure 0.3torr and 1hour.

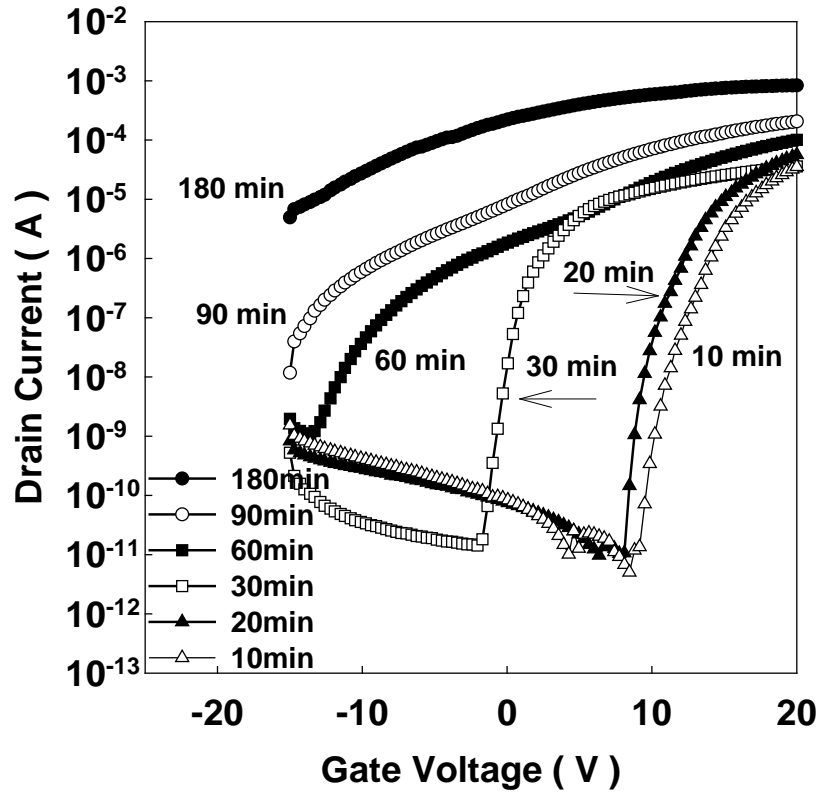


Fig. 3.17 The transfer characteristic with different UV lamp illumination time (10~180 min).

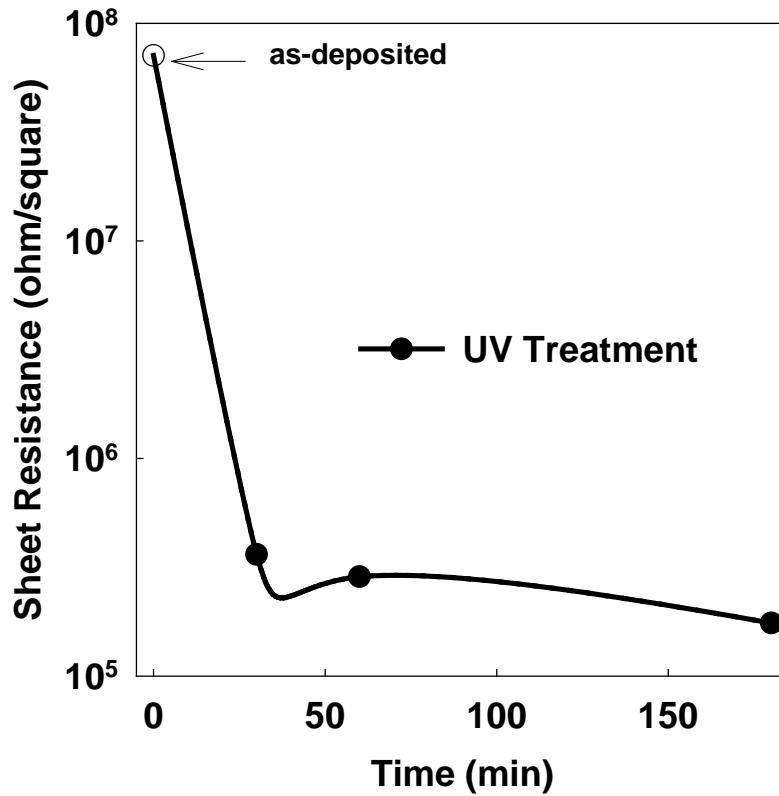


Fig. 3.18 The sheet resistance with different UV lamp illumination time (10~30 min).

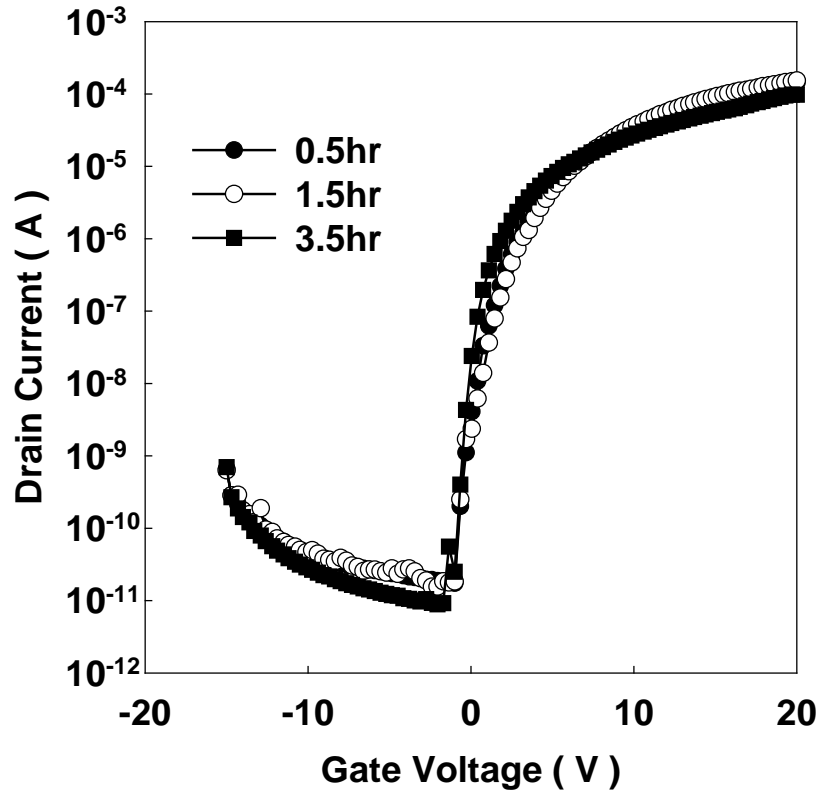


Fig. 3.19 The transfer characteristic with different pulse laser energy treatment after furnace annealing 400°C, O₂ flow 120 sccm, pressure 0.3torr and 1hour.

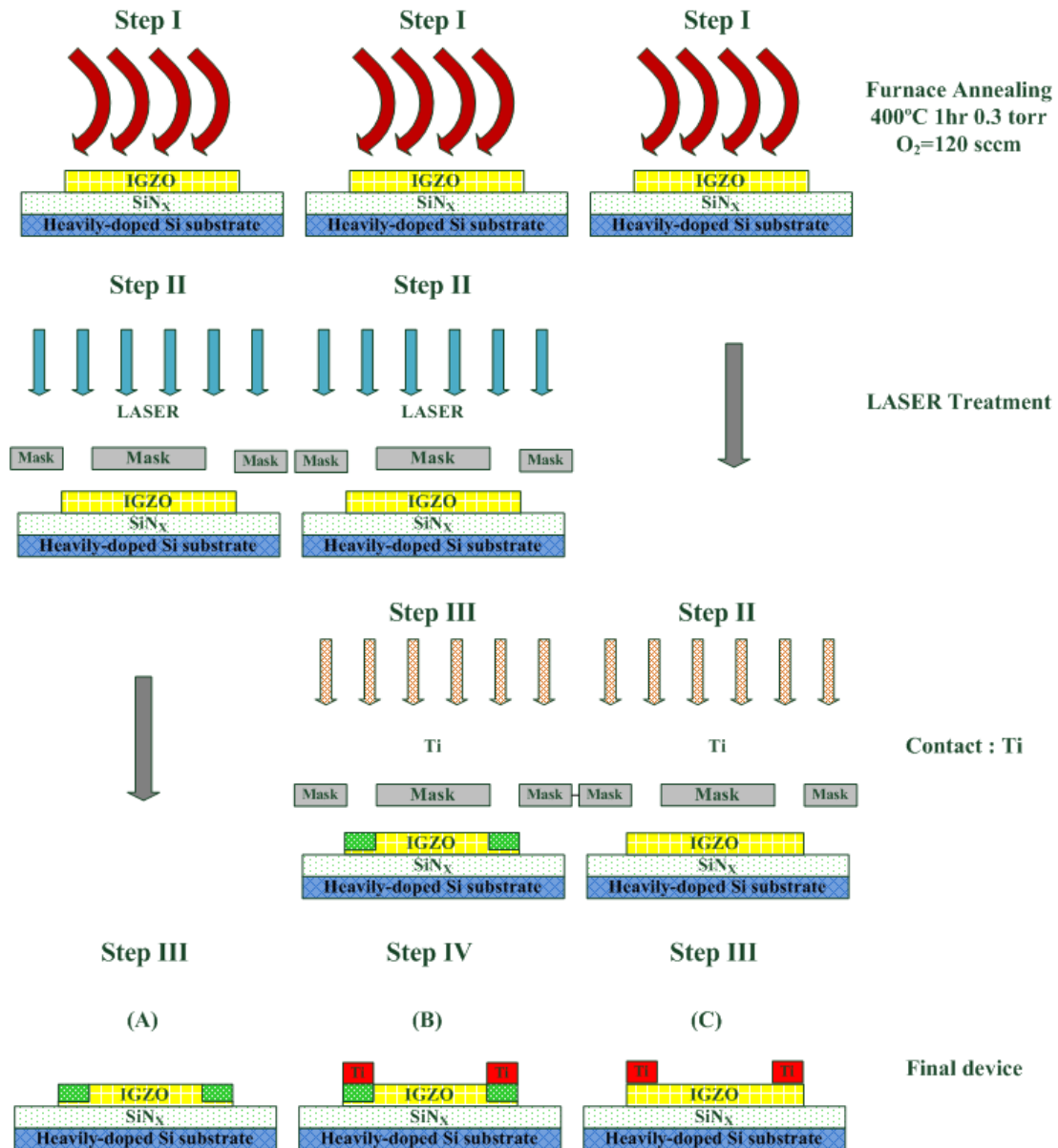


Fig. 3.20 The flow charts that present the light pattern procedure. Sample (A) represent the source/drain contacts were patterned by pulse laser illumination directly of the first a-IGZO TFTs. Sample (B) equipped with Ti pads on the area treated by pulse laser previously to form the source/drain contact. Ti pads serve as source/drain contacts in the third IGZO TFT which denoted by Sample (C).

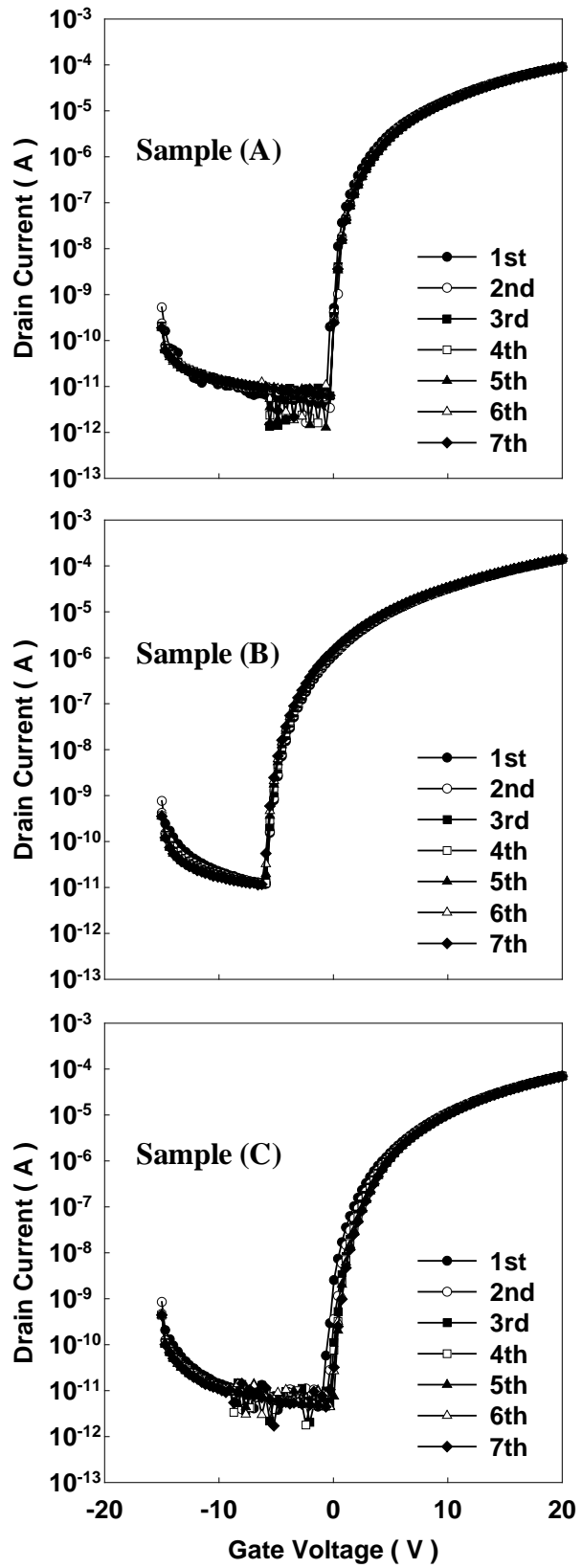


Fig. 3.21 The transfer characteristic of sample (A), (B) and (c).

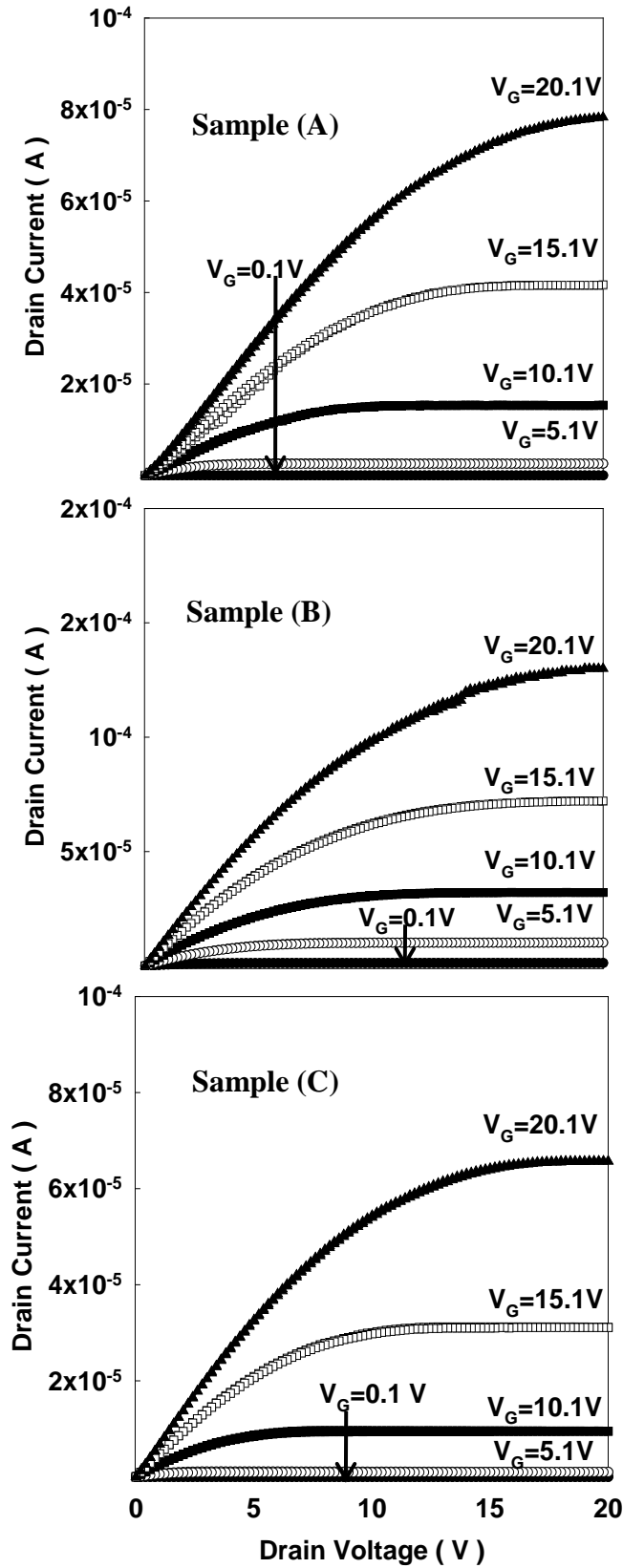


Fig. 3.22 The output characteristic of sample (A), (B) and (C).

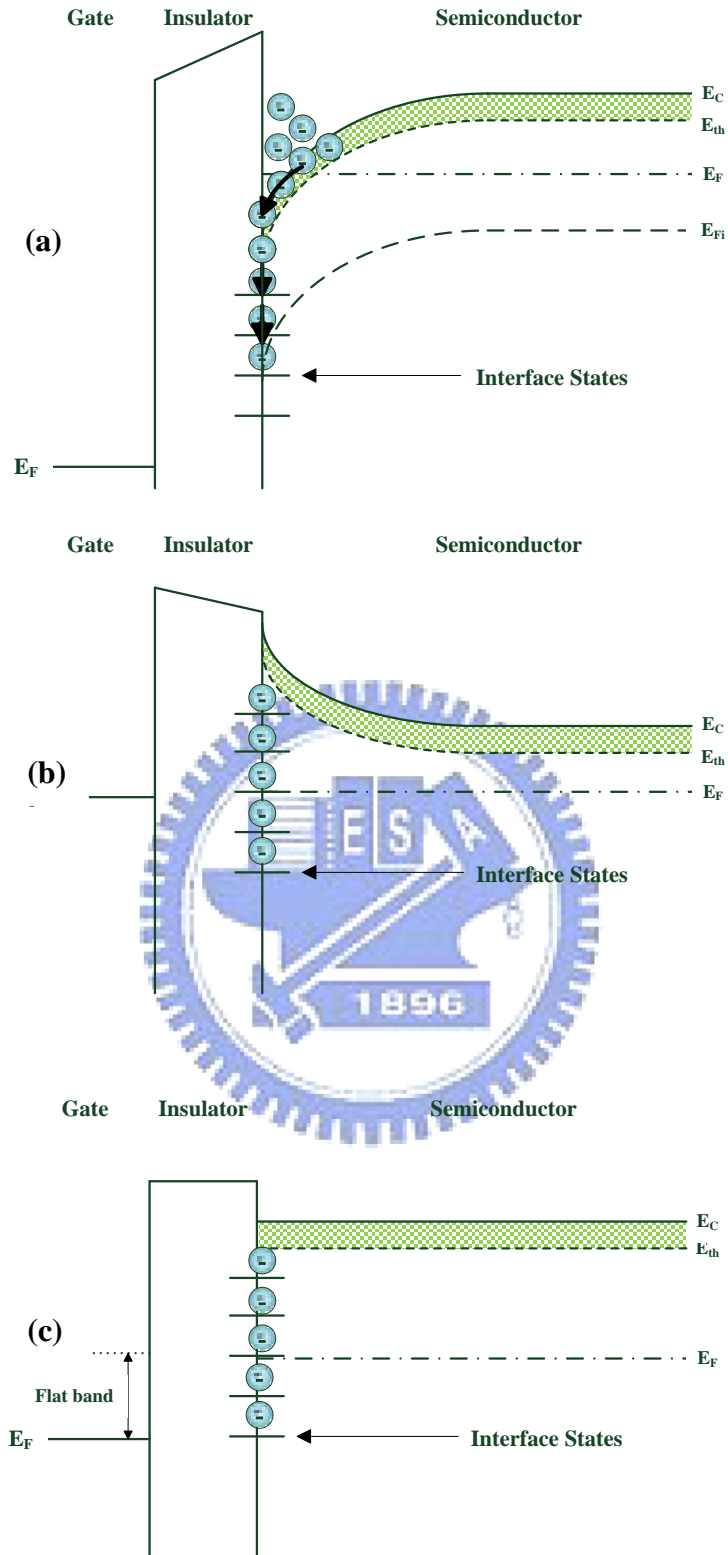


Fig. 3.23 The trapping mechanism of as-fabricated a-IGZO TFTs. (a) The positive V_G that cause electron trapping between $\text{SiN}_x/\text{a-IGZO}$ interface. (b) After remove the bias, the trapped electrons were still not released. (c) During next measurement, the larger positive gate voltage is required to flat the conduction band.

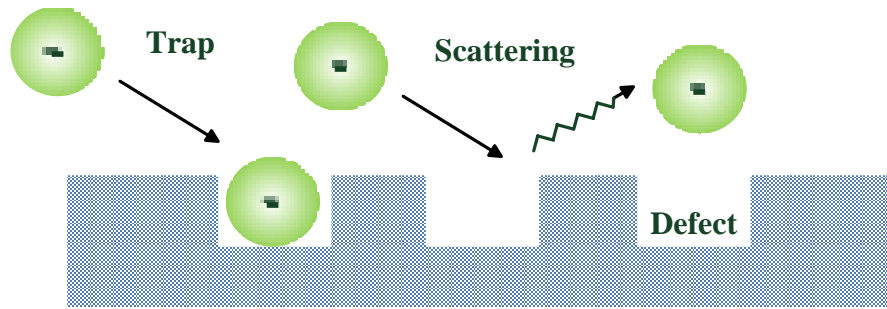


Fig. 3.24 The un-occupied defects that will make threshold shift and lower mobility by trapping and scattering the carrier, respectively.



Condition	V_{TH} (V)	μ (cm^2/Vs)	S.S. (V/dec.)	On/Off
As-fabricated	11.1	13.12	0.2	5.80×10^7
Furnace annealing 300C in N2	2.8	9.54	0.1	3.80×10^8
Furnace annealing 350C in N2	1.8	6.51	0.95	4.30×10^8
Pulse laser	0.3	6.23	0.32	1.60×10^7
UV	0.2	3.49	0.71	2.50×10^6

Table 3.1 The parameters of different post-annealing conditions

Energy Density (mJ/cm^2)	V_{TH} (V)	μ (cm^2/Vs)	S.S. (V/dec.)	On/Off
29.71	N/A	N/A	N/A	N/A
24.06	N/A	N/A	N/A	N/A
19.89	N/A	N/A	N/A	N/A
16.71	N/A	N/A	N/A	N/A
14.24	-7.8	1.94	1.69	2.10×10^5
12.28	2.2	2.16	1.49	1.30×10^6
10.69	0.3	6.23	0.32	1.60×10^7
10.02	12.6	9.46	0.12	6.50×10^7

Table 3.2 The parameters of different pulse laser energy density

Time (min)	V_{TH} (V)	μ (cm^2/Vs)	S.S. (V/dec.)	On/Off
180	N/A	N/A	N/A	N/A
90	N/A	N/A	N/A	N/A
60	N/A	N/A	N/A	N/A
30	0.2	3.49	0.71	2.50×10^6
20	11.3	11.51	0.35	5.30×10^6
10	12.9	10.88	0.75	7.00×10^6

Table 3.3 The parameters of different UV lamp illumination time

Sample	V_{TH} (V)	μ (cm^2/Vs)	S.S. (V/dec.)	On/Off
 (A)	2.7	8.07	0.22	1.4×10^7
 (B)	0.4	9.78	0.61	1.3×10^7
 (C)	3.3	6.85	0.6	1.6×10^7

Table 3.4 The parameters of different UV lamp illumination time

Chapter 4

Conclusions and Future Work

4-1 Conclusions

In this thesis, we reported the low temperature annealing method based on pulse laser and UV lamp illumination. Flexible electronics is one of most attractive subjects recently. Almost flexible substrate is temperature limited that motivated us to develop a low temperature fabricatable transistor. Pulse laser and UV lamp were demonstrated in this study to execute effective post-annealing. Except the advantage of low temperature, the timesaving is also possible. The required exposure times for one single a-IGZO TFTs by pulse laser was few seconds, pulse is suitable to treat a local area. UV lamp could provide a widely homogeneous radiation that is suitable for mass production. The required exposure time for UV lamp based annealing process is around tens of minutes. Moreover, UV lamp is economic for manufacture. By our experiments, we demonstrate the performance of a-IGZO TFTs annealed by light illumination is comparable with the one treated with furnace annealing at the temperature of more than 300°C for a period of at least 1 hour. The possible mechanism to explain the feasibility of annealing is that the disordered structure was improved by re-arranging the atoms in a-IGZO channel layer and then reducing trapping defects during annealing process. Thus, annealing could improve

performance, stability especially.

Besides, we demonstrate that the pulse laser also could be employed to improve the contact or pattern the S/D region directly. The devices subjected the pulse laser treatment perform better by the reduced contact resistance due to conductive a-IGZO film.

4-2 Future Work

The developed techniques in this study could provide a base to pursuit further device structure. The stable transistors on temperature limited flexible substrate could be developed based on the light annealing process.

The top-gate self-aligned thin film transistor patterned by light illumination is an attractive structure for electronic technology. Top-gate self-aligned structure could reduce the use of mask and also minimize the parasitic capacitance by reducing the overlap of gate electrode. Light pattern is potential to replace the expensive ion implantation and simplify the fabrication process.

Reference

- [1] H.A. Klasens and H. Koelmans, Solid State Electron, **7** (1964) 701.
- [2] M. Oritay, H. Ohta, M. Hirano, S. Narushima and H. Hosono, Philosophical magazine B, **81** (2001) 501.
- [3] S. Masuda, K. Kitamura, Y. Okumura, S. Miyatake, H. Tabata, T. Kawai, J. Appl. Phys., **93** (2003) 1624.
- [4] R. L. Hoffman, B. J. Norris, J. F. Wager, Appl. Phys. Lett., **82** (2003)733.
- [5] W. B. Jackson, R. L. Hoffman, G. S. Herman, Appl. Phys. Lett., **87** (2005) 193503.
- [6] N. L. Dehuff, E. S. Kettenring, D. Hong, H. Q. Chiang, J. F. Wager, R. L. Hoffman, C. -H. Park, D. A. Keszler, J. Appl. Phys. **97** (2005) 064505.
- [7] K. Nomura, H. Ohta, A. Takagi, T. Kamiya, M. Hirano, H. Hosono, Nature, **432** (2004) 488.
- [8] K. Nomura, H. Ohta, K. Ueda, T. Kamiya, M. Hirano, H. Hosono, Microelectronic Engineering, **72** (2004) 294.
- [9] H. Yabuta, M. Sano, K. Abe, T. Aiba, T. Den, H. Kumomi, K. Nomura, T. Kamiya, H. Hosono, Appl. Phys. Lett. **89** (2006) 112123.
- [10] Y. Sun and J. A. Rogers, Adv. Mater., **19** (2007) 1897.
- [11] D. Y. Ku, I. H. Kim, I. Lee, K. S. Lee, T. S. Lee, J. -h. Jeong, B. Cheong, Y. -J.

- Baik, W. M. Kim, **515** (2006) 1364.
- [12] H. Kumomi, K. Nomura, T. Kamiya, and H. Hosono, *Thin Solid Films* **516** (2008) 1516.
- [13] H. Hosono, K. Nomura, Y. Ogo, T. Uruga, and T. Kamiya, *J. Non-Cryst. Solids* **354** (2008) 2796.
- [14] W.B. Jackson, R.L. Hoffman, G.S. Herman, *Appl. Phys. Lett.* **87** (2005) 193503.
- [15] P. Görrn, M. Sander, J. Meyer, M. Kröger, E. Becker, H.-H. Johannes, W. Kowalsky, T. Riedl, *Adv. Mater.* **18** (2006) 738.
- [16] W. Lim, D.P. Norton, J.H. Jang, V. Craciun, S.J. Pearton, and F. Ren, *Appl. Phys. Lett.* **92** (2008) 122102.
- [17] R. L. Hoffman et al., *Appl. Phys. Lett.* **82** (2003) 733.
- [18] H.Q. Chiang, B.R. McFarlane, D. Hong, R.E. Presley, and J.F. Wager, *J. Non-Cryst. Solids* **354** (2008) 2826.
- [19] K. Nomura, H. Ohta, A. Takagi, T. Kamiya, M. Hirano and H. Hosono, *Nature*, **288** (2004) 432.
- [20] M. Oritay, H. Ohta, M. Hirano, S. Narushima and H. Hosono, *Philosophical magazine*, **B81** (2001) 501.
- [21] Mott, N. F. Silicon dioxide and the chalcogenide semiconductors; similarities

and differences. *Adv. Phys.*, **26** (1977) 363.

- [22] Narushima, S. et al. Electronic structure and transport properties in the transparent amorphous oxide semiconductor $2\text{CdO}\cdot\text{GeO}_2$. *Phys. Rev. B*, **66** (2002) 35203.
- [23] Orita, M. et al. Amorphous transparent conductive oxide $\text{InGaO}_3(\text{ZnO})_m$ ($m \leq 4$): a Zn 4s conductor. *Phil. Mag.* **81** (2001) 501.
- [24] Tatsuya Iwasaki, Naho Itagaki, Tohru Den, Hideya Kumomi, Kenji Nomura, Toshio Kamiya, and Hideo Hosono *Appl. Phys. Lett.*, **90** (2007) 242114.
- [25] P. Barquinha, L. Pereira, G. Gonçalves, R. Martins, and E. Fortunato, *Journal of The Electrochemical Society*, **156** (2009) 161-168.
- [26] T. Kamiya, H. Hiramatsu, K. Nomura, and H. Hosono, *J. Electroceram.*, **17** (2006) 267.
- [27] H. Hosono, *J. Non-Cryst. Solids*, **352** (2006) 851.
- [28] H. C. Pan, M. H. Shiao, C. Y. Su, and C. N. Hsiao, *J. Vac. Sci. Technol.* **23** (2005) 1187.
- [29] R. Martins, P. Barquinha, I. Ferreira, L. Pereira, G. Goncalves, and E. Fortunato, *J. Appl. Phys.*, **101** (2007) 044505.
- [30] Kenji Nomura, Akihiro Takagi, Toshio Kamiya, Hiromichi Ohta, Masahiro Hirano and Hideo Hosono, *Japanese Journal of Applied Physics*, **45** (2006)

4303–4308.

- [31] Mitsuru Nakata, Kazushige Takechi, Kazufumi Azuma¹, Eisuke Tokumitsu, Hiroataka Yamaguchi, and Setsuo Kaneko, *Applied Physics Express*, **2** (2009) 021102.
- [32] B. D. Ahn, H. S. Shin, W. H. Jeong, G. H. Kim, H. J. Kim, S. H. Choi, M. K. H, *SID*, **3903** (2009) 1170.
- [33] J. K. Jeong, J. H. Jeong, H. W. Yang, J.-S. Park, Y.-G. Mo, and H. D. Kim, *Appl. Phys. Lett.*, **91** (2007) 113505.
- [34] W. Lim, S.-H. Kim, Y.-L. Wang, J. W. Lee, D. P. Norton, S. J. Pearton, F. Ren, and I. I. Kravchenko, *J. Vac. Sci. Technol.*, **26** (2008) 959.
- [35] J.-S. Park, J. K. Jeong, Y.-G. Mo, H. D. Kim, and S.-I. Kim, *Appl. Phys. Lett.*, **90** (2007) 262106.
- [36] J. Park, L. Song, S. Kim, S. Kim, C. Kim, J. Lee, H. Lee, E. Lee, H. Yin, K. Kim, K. Kwon, and Y. Park, *Appl. Phys. Lett.*, **93** (2008) 053501.
- [37] Byung Du Ahn, Hyun Soo Shin, Hyun Jae Kim, Jin-Seong Park, and Jae Kyeong Jeong, *Appl. Phys. Lett.*, **693** (2008) 20350
- [38] Wantae Lim, Jung Hun Jang, S.-H. Kim, D. P. Norton, V. Craciun, and S. J. Pearton, F. Ren, H. Chen, *J. Vac. Sci. Technol.* **27** (2009) 126.
- [39] D. K. Schroder, *Semiconductor Material and Device Characterization*. New York,

New York: John Wiley and Sons Inc., 2nd ed., (1998).

[40] K. N. Narayanan Unni, Sylvie Dabos-Seignon, and Jean-Michel Nunzi, J. Phys.

D: Appl. Phys., **38** (2005) 1148

[41] Hung Xiao, “Introduction to semiconductor manufacturing technology”,

International edition.

[42] J. E. Geusic et al., “Laser oscillations in Nd-doped yttrium aluminum, yttrium

gallium and gadolinium garnets”, Appl. Phys. Lett. **4** (1964) 182.

[43] Yukihiro Morimoto, Taku Sumitomo, Masaki Yoshioka, Tetsu Takemura, IA

(IEEE Industry application society) Annual Meeting, Sazuchi, Bessyo-cho,

Himeji, Japan, **1194** (2004) 6710224.

[44] A. Suresh, J. F. Muth, USA, Appl. Phys. Lett., **92** (2008) 033502.

[45] Hyun Soo Shin , Byung Du Ahn , Kyung Ho Kim , Jin-Seong Park , Hyun Jae

Kim, Thin solid Films, **25793** (2009) 4.

[46] Jong Han Jeong, Hui Won Yang, Jin-Seong Park, Jae Kyeong Jeong, Yeon-Gon

Mo, Hye Dong Kim, Jaewon Song, and Cheol Seong Hwang, Electrochemical

and Solid-State Letters, **11** (2008) 157.

[47] Donghun Kang, Hyuck Lim, Changjung Kim, Ihun Song, Jaechoel Park,

Youngsoo Park, JaeGwan Chung, Appl. Phys. Lett. **90** (2007) 192101.

[48] Donghun Kang, Ihun Song, Changjung Kim, and Youngsoo Park, Tae Dong

Kang, Ho Suk Lee, Jun-Woo Park, Seoung Ho Baek, Suk-Ho Choi, and Hosun

Lee, Appl. Phys. Lett. **91** (2007) 091910.

[49] Mami FUJII, Hiroshi YANO, Tomoaki HATAYAMA, Yukiharu URAOKA,

Takashi FUYUKI, Ji Sim JUNG, and Jang Yeon KWON, Japanese Journal of

Applied Physics **47** (2008) 6236.

[50] B. D. Ahn, H. S. Shin, W. H. Jeong, G. H. Kim, H. J. Kim, S. H. Choi, M. K. H,

SID, **3903** (2009) 1170.

[51] T. Akane, K. Sugioka, K. Midorikawa, J. Vac. Sci. Technol., **18** (2000) 1406.

[52] H. W. Jang, T. Sands, J.-L. Lee, J. Appl. Phys., **94** (2003) 3529

[53] H.-J. Chung, J. H. Jeong, T. K. Ahn, H. J. Lee, M. Kim, K. Jun, J.-S. Park, J. K.

Jeong, Y.-G. Mo, and H. D. Kim: Electrochem. Solid-State Lett. **11** (2008) 51.

[54] R. C. Ross and R. Messier, J. Appl. Phys., **52** (1981) 5329.



Resume

基本資料:

姓名:黃慶能

出生日期:中華民國 72 年 08 月 13 日

住址:桃園縣平鎮市育達路 228 號 9 樓之 1

學歷:

私立逢甲大學航空工程學系 (2001. 9~2003. 6)

國立交通大學機械工學學系 (2003. 9~2006. 6)

國立交通大學光電工程研究所碩士 (2007. 9~2009. 7)



論文題目:

IGZO 薄膜電晶體之光學低溫退火與金屬接觸界面處理

Development of Low Temperature Annealing and Contact treatment

by Light Illumination on Amorphous Indium-Gallium-Zinc-Oxide

(a-IGZO) Thin Film Transistor